Cell

Article

Structure of gut microbial glycolipid modulates host inflammatory response

Graphical abstract

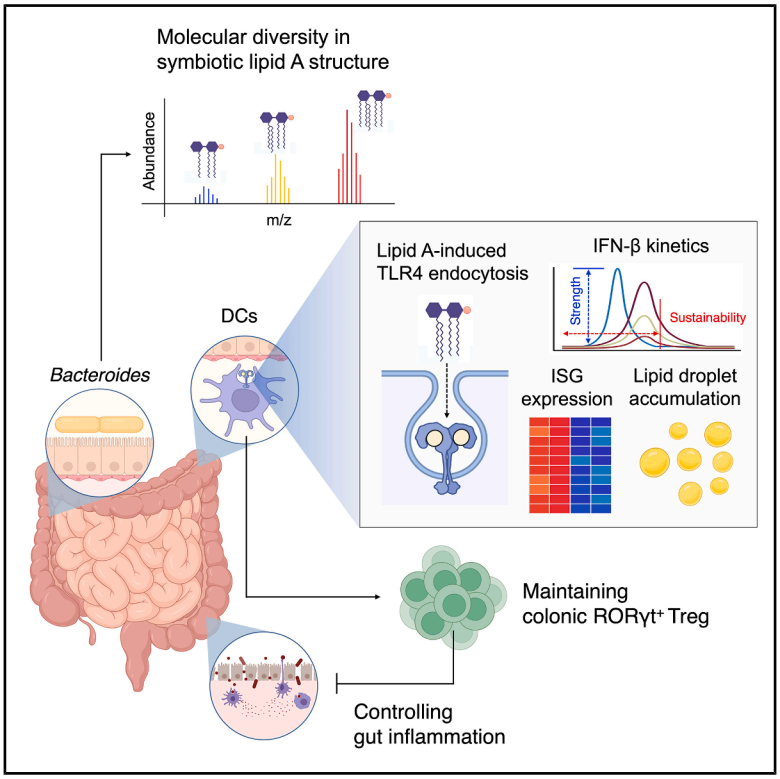

Highlights

- Symbiont lipid A molecular structures vary in the degree of acylation/phosphorylation
- Structural variations in lipid A impact greatly on IFN-β response via IFNAR
- Lipid A-induced IFN-β responses rely on TLR4 endocytosis and lipid droplet formation
- Lipid A structure modulates gut inflammation via induction of RORγt^{+} Treg

Authors

Hyoung-Soo Cho, Ji-Sun Yoo, Xinyang Song, ..., Seung Bum Park, Sungwhan F. Oh, Dennis L. Kasper

Correspondence

hyoung-soo_cho@hms.harvard.edu (H.-S.C.), dennis_kasper@hms.harvard.edu (D.L. K.)

In brief

Structural variations in the number of acyl chains and phosphate groups of gram-negative microbial lipid A differentially modulate DC-derived IFN-β responses, which are mechanistically regulated by TLR4 endocytosis and lipid droplet formation. This lipid A-structure-driven immunomodulation via IFN-β contributes to the maintenance of colonic RORγt^{+} Tregs during homeostasis and helps mitigate colonic inflammation.

Cho et al., 2025, Cell *188*, 1–18
September 18, 2025
https://doi.org/10.1016/j.cell.2025.05.016

CellPress

Cell

CellPress

Article

Structure of gut microbial glycolipid modulates host inflammatory response

Hyoung-Soo Cho,[1,*] Ji-Sun Yoo,[2] Xinyang Song,[1] Byoungsook Goh,[2] Alos Diallo,[1] Jesang Lee,[3] Sumin Son,[3] Yoon Soo Hwang,[3] Seung Bum Park,[3] Sungwhan F. Oh,[2,4] and Dennis L. Kasper[1,5,*]

[1]Department of Immunology, Harvard Medical School, Boston, MA 02115, USA

[2]Department of Anesthesiology, Perioperative and Pain Medicine, Center for Experimental Therapeutics and Reperfusion Injury, Brigham and Women's Hospital, Boston, MA 02115, USA

[3]Department of Chemistry, CRI Center for Chemical Proteomics, Seoul National University, Seoul, Republic of Korea

[4]Program in Immunology, Division of Medical Sciences, Harvard Medical School, Boston, MA 02115, USA

[5]Lead contact

*Correspondence: hyoung-soo_cho@hms.harvard.edu (H.-S.C.), dennis_kasper@hms.harvard.edu (D.L.K.)

https://doi.org/10.1016/j.cell.2025.05.016

SUMMARY

Commensals are constantly shaping the host's immunological landscape. Lipopolysaccharides found in gram-negative microbes have a terminal lipid A in their outer membrane. Here, we report that structural variations in symbiotic lipid A lead to divergent immune responses with each lipid A structure, eliciting effects distinct from those induced by classical lipid A. Certain lipid A structures can induce a sustained interferon (IFN)-β response orchestrated by Cdc42-facilitated Toll-like receptor 4 (TLR4) endocytosis and lipid droplet (LD) formation. This lipid A-directed IFN-β response is paramount for colon RORγt$^+$ regulatory T cell (Treg) induction while simultaneously suppressing colonic T_H17 cells and controlling gut inflammation. Intriguingly, the quantitatively dominant penta-acylated lipid A species in Bacteroidetes fails to elicit an IFN-β response. Instead, a less abundant tetra-acylated lipid A species sustainably induces IFN-β, thereby contributing to RORγt$^+$ Treg homeostasis. Nuances in symbiont lipid A structure contribute to maintaining potent regulation of Tregs to maintain a healthy endobiotic balance.

INTRODUCTION

A range of microbial products shape the host immunological landscape.[1–5] Although symbiotic microbes produce molecules that trigger protective responses against pathogens,[6–8] they also produce immunomodulatory molecules that maintain immune homeostasis and prevent autoimmunity.[9–13] Recent advances have uncovered an intricate relationship between symbiotic microbes and host immunity.[14,15] Regulatory T cells (Tregs) play a crucial role in controlling deleterious inflammation, and accumulating evidence indicates the microbiota profoundly influence this subset.[16–18] Yet, the diversity and complexity of the host microbiota have made it challenging to unravel the underlying mechanisms responsible for microbiota-induced immunomodulation.

Gram-negative bacteria have an outer membrane glycolipid called lipopolysaccharides (LPSs) or lipooligosaccharides (LOSs, LPS without O-antigen). Both LPS and LOS comprise a carbohydrate core linked to a terminal lipid A anchoring these molecules into the outer membrane. Lipid A is the endotoxic component of LPS from pathogenic microbes responsible for inducing proinflammatory responses.[19,20] However, the lipid A moieties from the LOS of Bacteroidetes occupying 40%–60% of human gut microbiota are only marginally proinflammatory and have, in fact, been associated with immunomodulatory functions.[21,22] *Bacteroides fragilis* possesses a surface polysaccharide called PSA that exhibits potent immunomodulatory activity by stimulating DCs to produce interferon (IFN)-β and/or inducing interleukin (IL)-10 from Tregs.[7,11,23]

Toll-like receptor 4 (TLR4) is a pivotal receptor for innate immune recognition of glycolipids from gram-negative bacteria, and its diverse downstream signaling is dictated by the location of TLR4, either on the surface or within the endosome.[24–28] TLR4-mediated signaling triggered at the cell surface is modulated by TIRAP and MyD88.[29,30] On the other hand, upon endocytosis of TLR4-MD2 complexed with glycolipids, endosomal TLR4 signaling, mediated exclusively by TRAM and TRIF, directly activates type I IFNs.[27,28,31,32] Although the molecular mechanisms of TLR4 endocytosis and its downstream signaling driven by *E. coli* LPS have been investigated, the impact of structural variations in symbiotic lipid A on TLR4-mediated immune recognition remains unexplored.

Compared with conventional lipid A, symbiotic lipid A displays greater molecular diversity and complexity.[22,33] Although the conventional lipid A of pathogenic LPS is uniformly hexa-acylated and diphosphorylated, the structure of symbiotic lipid A is more variable, characterized by fewer and longer acyl chains and a single phosphate group. A few studies have

Please cite this article in press as: Cho et al., Structure of gut microbial glycolipid modulates host inflammatory response, Cell (2025), https://doi.org/10.1016/j.cell.2025.05.016

shown that structural diversity in lipid A affects the susceptibility of commensals to anti-microbial peptides and impacts on their immunomodulatory activities.[22,34] However, whether this molecular diversity in symbiotic lipid A modulates host immune responses differently from conventional lipid A remains unresolved.

We examined the immunological effects of glycolipids containing natural lipid A and chemically synthesized lipid A analogs. We identified a distinct transcriptomic signature shaped by specific lipid A structures, notably linked to type I IFNs and IFN-stimulated genes (ISGs). We demonstrate a previously unappreciated mechanism by which lipid A structure influences the sustainability of IFN-β response, modulated by TLR4 endocytosis via Cdc42 and intracellular lipid droplet (LD) formation. Most importantly, lipid A-induced IFN-β responses promote the maintenance of colonic RORγt$^+$ Tregs, enabling persistent suppression of colonic T_H17 cells. Given the abundance of Bacteroidetes in human gut microbiota, we suggest that microbial lipid A structures are key determinants of intestinal immune homeostasis and host gut immunity.

RESULTS

Structural analogs of symbiotic lipid A exhibit variability in immunomodulatory potential against host inflammation

Lipidomic analysis of natural lipid A from *E. coli* and human gut symbiont *B. fragilis* revealed a striking contrast in their molecular attributes. The dominant natural lipid A structure found in *E. coli* is a diphosphorylated glucosamine disaccharide that is hexa-acylated (Figure 1A). The natural lipid A of *B. fragilis* is built on a monophosphorylated glucosamine disaccharide and is comprised of multiple structural variations having different numbers of acyl chains (Figure 1B). Detailed analysis of individual group acyl variants found in each microbe reveals that they are variable in their chain length (Table S1). Structural assignment of the most abundant chain length variant within each group (C82 in hexa-acylated and diphosphorylated [6A-DP] lipid A from *E. coli*; C81 in penta-acylated and monophosphorylated [5A-MP], C65 in tetra-acylated and monophosphorylated [4A-MP], and C49 in tri-acylated and monophosphorylated [3A-MP] lipid A from *B. fragilis*) confirms the molecular identity of represented lipid A species (Figures S1A–S1D).

The most abundant natural lipid A molecules found in *B. fragilis* LOS are the 5A- and 4A-MP (Figure 1B). We performed a comparative analysis using a set of synthetic lipid A analogs (s5A-MP-C80, s4A-MP-C64_1, and 2) (Figures S1E, S1G, and S1I; Table S2) that recapitulate the natural lipid A structure of *B. fragilis* (Figures S1B and S1C) in terms of location of acyl chains and phosphate group. As shown in MS/MS data, the lipidomic profile detected from the synthetic analog s5A-MP-C80 (Figure S1E) shows an identical fragmentation pattern to the natural 5A-MP lipid A structure in *B. fragilis* (n5A-MP-C81) (Figure S1F). Similarly, the fragmentation pattern displayed in MS/MS spectra of the s4A-MP-C64_1 and 2 (Figures S1G and S1I) confirms the presence of two isomeric natural 4A-MP lipid A structures (n4A-MP-C65_1 and 2) in *B. fragilis*, each having acyl chains in different positions (Figures S1H and S1J).

We found these natural lipid A variants challenging to individually purify from the organism due to their molecular similarity and the presence of multiple variants. To precisely assess the immunological activity of individual lipid A structures, we used a series of representative chemically synthesized lipid A analogs varying in their number of acyl chains of identical length (C14) and their phosphorylation status (Figure 1C). These synthetic lipid A analogs recapitulate Bacteroidetes lipid A structures, and 6A-DPLA is identical to lipid A from *E. coli*. To interrogate the impact of molecular variations in lipid A structure on host inflammation, we assessed the *in vivo* immunomodulatory potential of each lipid A synthetic analog in the dextran sodium sulfate (DSS)-induced colitis model. B6 wild-type (WT) mice were orally administered lipid A analogs for 4 days (day −3 to day 0) (Figure 1D), and the disease severity was evaluated by monitoring their weight changes upon DSS treatment. Mice treated with 4A-MPLA conferred the most effective protective response, as evidenced by reduced weight loss (Figure 1E) and improved colitis histopathology (Figure S1K). This protective response correlated with a reduced proportion of colitogenic cytokine-producing CD4$^+$ T cells in the colon (Figure 1F). Treatment with 3A-MPLA also ameliorated disease severity and abrogated the production of colitogenic cytokines. However, based on reduced IL-17A production by colonic CD4$^+$ T cells, 4A-MPLA exerted a more pronounced effect than any of the other lipid A analogs. In contrast to the immunomodulatory effects of 3A- and 4A-MPLA, 5A- and 6A-DPLA failed to mitigate weight loss or control colitogenic CD4$^+$ T cell response.

Structural variations in lipid A impacts upon the IFN-β response in DCs

To closely examine the impact of lipid A structural variations on immune responses, we treated mouse bone-marrow-derived DCs (mBMDCs) *in vitro* with these synthetic lipid A analogs and examined various cytokine responses after 24 h. Of the synthetic lipid A analogs, 6A-DPLA (structurally identical to the *E. coli* lipid A) induced the highest levels of all cytokines examined. The synthetic lipid A analogs with fewer acyl chains (3A- to 5A-MPLA) induced lower levels of all examined cytokines compared to the cytokine levels induced by 6A-DPLA. Among the lipid A analogs tested, 5A-MPLA was the weakest inducer of this group of cytokines. Of interest, the penta-acylated lipid A species, which is structurally correlated with 5A-MPLA, is most abundant in Bacteroidetes natural lipid A with a penta-acyl chain (Figure 1B).

Comparison of 3A- and 4A-MPLA demonstrated similar potencies in inducing proinflammatory cytokines (e.g., IL-6 and tumor necrosis factor alpha [TNF-α]) (Figures S2A and S2B), although 3A-MPLA induced modestly higher immunomodulatory cytokines (IL-10 and IFN-β) (Figures S2C and S2D). This relative magnitude of response to each lipid A analog is still retained over a range of lipid A concentrations (Figure S2E). Cytokine responses elicited by the LPS purified from *E. coli* (LPS-EC) are consistently higher than those induced by the LOS isolated from *B. fragilis* (LOS-BF). Although IL-6, TNF-α, and IL-10 responses to LOS-BF are higher than those induced by 3A- and 4A-MPLA, the comparative level of IFN-β induced by LOS-BF is quite similar. These results suggest that the natural

Please cite this article in press as: Cho et al., Structure of gut microbial glycolipid modulates host inflammatory response, Cell (2025), https://doi.org/10.1016/j.cell.2025.05.016

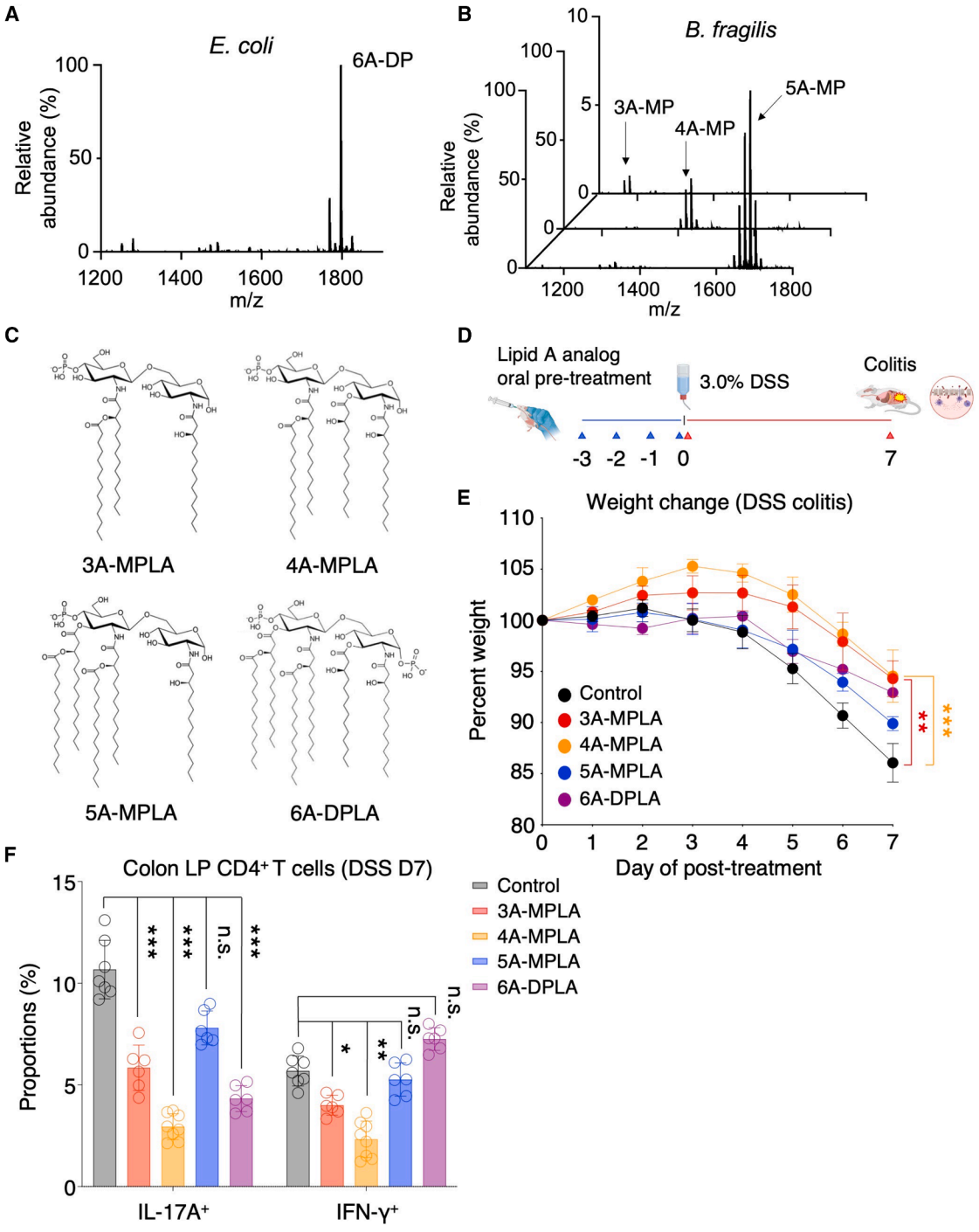

Figure 1. Structural analogs of symbiotic lipid A exhibit variability in immunomodulatory potential against host inflammation

(A and B) Structural analyses of lipid A from *E. coli* Nissle 1917 (A) and *B. fragilis* NCTC 9343 (B) via liquid chromatography-mass spectrometry (LC-MS). 3A-MP, tri-acylated and monophosphorylated; 4A-MP, tetra-acylated and monophosphorylated; 5A-MP, penta-acylated and monophosphorylated; 6A-DP, hexa-acylated and diphosphorylated.

(C) Molecular structure of synthetic lipid A analogs.

(D–F) Oral treatment regimen of synthetic lipid A analogs (20 μg/day from day −3 to day 0, total 80 μg/mouse) and DSS (3.0%, day 0 to day 7) to SPF B6 WT mice for colonic inflammation model (D). Immunoprotective effect of oral administration of synthetic lipid A analogs on DSS-induced colonic inflammation determined by weight changes during DSS treatment (E) and colitogenic cytokine production (IL-17A and IFN-γ) from colon LP $CD4^+$ T cells (F).

n.s., not significant; $^*p < 0.05$; $^{**}p < 0.01$; $^{***}p < 0.001$, unpaired/paired Student's t test. Error bars represent mean ± SEM.

See also Figure S1 and Tables S1 and S2.

Please cite this article in press as: Cho et al., Structure of gut microbial glycolipid modulates host inflammatory response, Cell (2025), https://doi.org/10.1016/j.cell.2025.05.016

lipid A species found in *B. fragilis* and the synthetic 3A- and 4A-MPLA, which share structural similarities in acyl chain number and phosphorylation degree, exhibit similar capacities to induce IFN-β.

We also examined whether the difference in phosphate group position of the lipid A affects the activity of monophosphorylated lipid A by synthesizing structural analogs with identical numbers of acyl chains and phosphate groups located at a different position (C1 vs. C4′) (Figures S1E and S2F; Table S2). Despite structural differences, the ability to induce IFN-β from mBMDCs was comparable across each pair of analogs (Figure S2G). We also found that the tetra-acylated lipid A isomer analogs (4A-MPLA vs. s4A-MP_C68) similarly mitigated colonic inflammation induced by DSS treatment (Figure S2H).

To elucidate the impact of lipid A structure on innate immune signaling, we incubated synthetic lipid A analogs with mBMDCs derived from several transgenic mouse strains with genetic deficiencies in critical innate immune receptors (*Tlr4*$^{-/-}$ and *Tlr2*$^{-/-}$) and their downstream adapter molecules (*Myd88*$^{-/-}$ and *Ticam1*$^{-/-}$). As expected, TLR4 and TRIF are both necessary for all lipid A synthetic analogs to stimulate production of IL-6, TNF-α, IL-10, and IFN-β. However, none of the lipid A synthetic analogs that we tested require TLR2 for the induction of these cytokines. All lipid A varieties require MyD88 for the induction of IL-6, TNF-α, and IL-10 (Figures 2A–2C). 5A-MPLA is broadly inactive in induction of any of these cytokines, regardless of genetic backgrounds of DCs. Upon stimulation with 3A- or 4A-MPLA, a higher IFN-β response was induced by *Myd88*$^{-/-}$ DCs when compared with the response induced by WT DCs. In contrast, stimulation with 6A-DPLA resulted in a lower IFN-β response in *Myd88*$^{-/-}$ DCs than observed in WT DCs (Figure 2D). Because IFN-β induction is dependent on TRIF-mediated signaling, these data suggest that 3A- and 4A-MPLA are more likely to engage with endosomal TLR4, thereby signaling through TRIF to induce IFN-β.

Next, we further investigated how the structures of molecular analogs of lipid A influence their relative binding affinity to TLR4-MD2 complex. Across a range of concentrations, 5A-MPLA exhibited the weakest affinity to this complex, consistent with its minimal cytokine activity in DCs. In contrast, 6A-DPLA displayed the strongest affinity to this complex. Intriguingly, 4A-MPLA displayed binding affinity comparable to 6A-DPLA, and this affinity was significantly higher than that of 3A- and 5A-MPLA (Figure 2E).

To determine the functional impact of lipid A structure on the immune system more comprehensively, we analyzed the transcriptomic signature of DCs treated with synthetic lipid A analogs via bulk RNA sequencing (RNA-seq). The principal-component analysis (PCA) of entire DC transcriptome data revealed that the molecular variations in acylation/phosphorylation of lipid A structure modulate DCs to exhibit distinguishable signatures (Figure 2F). These data suggest that lipid A structure is a critical determinant dictating immunomodulatory activity of commensal microbial lipid A. Pathway enrichment analysis of differentially expressed genes (DEGs) following DC activation by different lipid A structures revealed that genes most strongly upregulated by 3A- or 4A-MPLA were primarily associated with ISGs, type I IFN signaling, and cell-cycle regulators involved in IFN-β translation (e.g., CDK1, cyclin B1) (Figures 2G and S3A; Table S3).[35,36] In contrast, 5A-MPLA and other lipid A analogs did not exhibit any such activity. On the other hand, the most enriched pathways associated with downregulated transcriptomic signature induced by 3A- or 4A-MPLA are those associated with lysosome/phagosome or cross presentation (e.g., cathepsin B, v-ATPase, or Cd36) (Figure S3B; Table S4).

IFN-β response to lipid A structure is mediated by the degree of TLR4 endocytosis and LD biogenesis

Our transcriptome analyses enriched with the genes associated with type I IFNs were based on changes in DCs after 24 h. We further examined the kinetics of lipid A-induced IFN-β response by examining *Ifnb* mRNA expression by q-PCR after incubating mBMDCs with 4 different synthetic lipid A analogs at different time points. The level of *Ifnb* mRNA expression induced by 6A-DPLA was consistently higher than the level induced by 3A- or 4A-MPLAs until 12 h. Of interest, the level of *Ifnb* mRNA expression induced by 3A- or 4A-MPLA remained elevated compared with baseline at 24 and 36 h, but the *Ifnb* mRNA expression induced by 6A-DPLA was precipitously reduced at these later time points. Consistent with its weak binding to TLR4-MD2 and lack of cytokine activity, 5A-MPLA did not induce substantial *Ifnb* mRNA expression. Among the tested lipid A analogs, 4A-MPLA induced the most sustained IFN-β response in DC, lasting up to 36 h (Figure 3A). Supporting these *Ifnb* mRNA expression kinetics, the protein level of IFN-β being accumulated in mBMDC culture is rapidly induced by 6A-DPLA stimulation. 6A-DPLA induced the highest levels of IFN-β at early time points compared with the IFN-β levels induced by 3A- or 4A-MPLA at the same time points (Figure S4A). In contrast to the kinetics of *Ifnb* mRNA levels, *Il6* mRNA expression levels induced by 3A- and 4A-MPLA were consistently lower than those induced by 6A-DPLA across all time points (Figure S4B).

Our *in vitro* data demonstrated that specific lipid A structures impact the transcriptome associated with type I IFNs and revealed the prolonged nature of lipid A-directed TLR4 signaling by 3A-MPLA and, especially, by 4A-MPLA. To examine whether these structure-driven changes in type I IFN response are observable *in vivo*, we utilized IFNβ1-EYFP reporter mice to monitor IFN-β production by colonic DCs. Among various DC subsets, we confirmed that IFN-β production and *Ifna* mRNA expression are most pronounced in pDCs residing in the colonic lamina propria (LP) (Figures S4C–S4F). Interestingly, as we previously demonstrated,[17] the colonic pDC subset is highly sensitive to the presence of gut microbes. Supporting this, the depletion of gut microbiota markedly reduced the proportion of colonic pDCs and their production of IFN-β, whereas other DC subsets remained unaffected (Figures S4G and S4H). Therefore, we focused on changes in the colonic pDCs following gavage of lipid A synthetic analogs to the IFNβ1-EYFP reporter mice. *In vivo* IFN-β response by colonic pDCs began to increase from baseline as early as 6 h after treatment with either 4A-MPLA or 6A-DPLA. These two analogs induced comparable levels of IFN-β in colon pDCs, whereas 3A-MPLA elicited no response at this time point. The IFN-β response stimulated by 6A-DPLA precipitously resolved after 12 h, whereas the IFN-β response induced by 3A- and 4A-MPLA peaked at 12 h but remained high until 18 h post oral treatment (Figure 3B). These *in vivo* results are

Please cite this article in press as: Cho et al., Structure of gut microbial glycolipid modulates host inflammatory response, Cell (2025), https://doi.org/10.1016/j.cell.2025.05.016

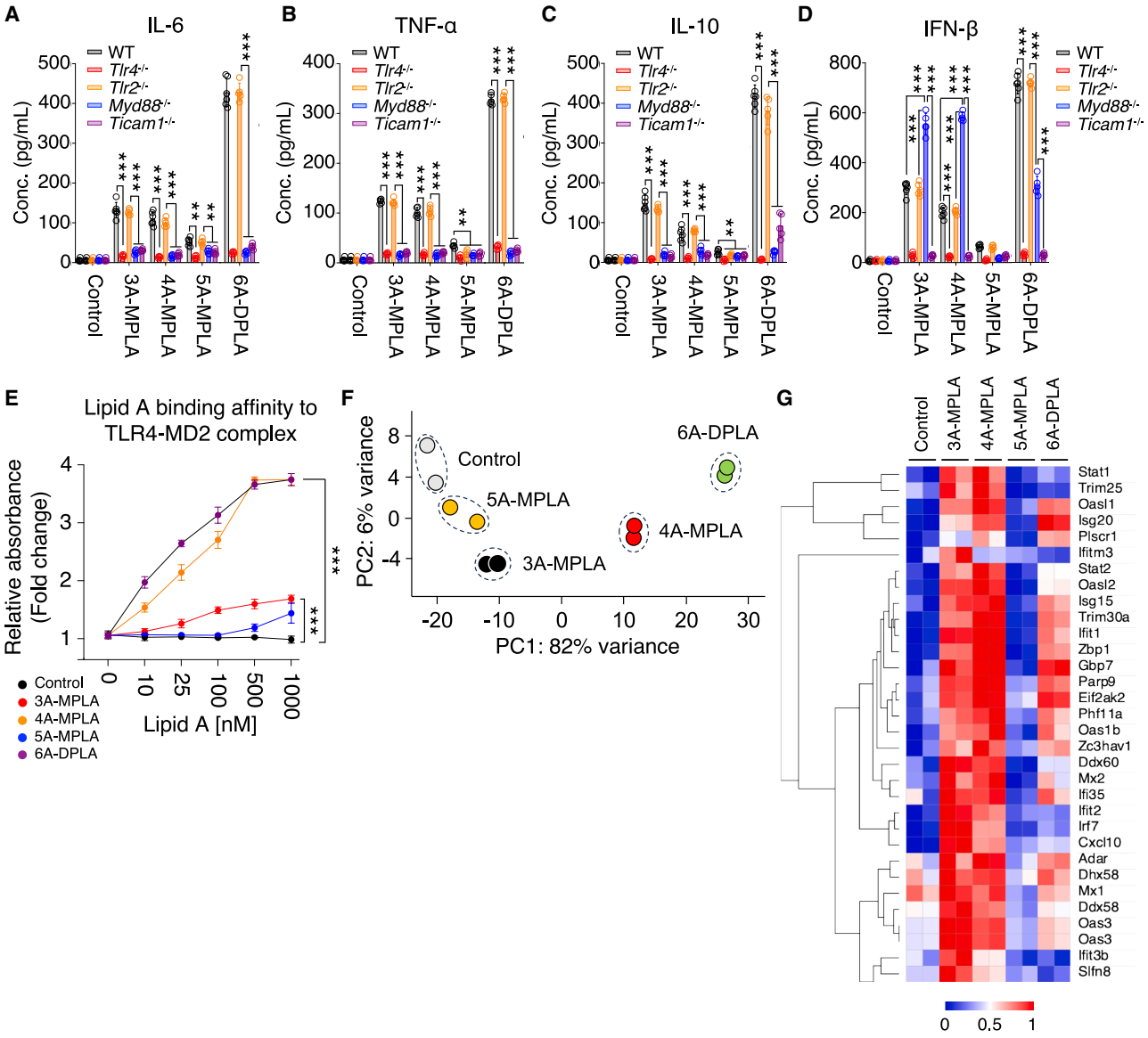

Figure 2. Structural variations in lipid A impacts upon the IFN-β response in DCs

(A–D) Cytokine responses (IL-6, TNF-α, IL-10, and IFN-β) of mBMDCs derived from WT, *Tlr4*$^{-/-}$, *Tlr2*$^{-/-}$, *Myd88*$^{-/-}$, and *Ticam1*$^{-/-}$ mice stimulated by different synthetic lipid A analogs (1.0 μg/mL).

(E) Relative binding affinity of synthetic lipid A analogs to human TLR4-MD2 complex.

(F) Principal-coordinate analysis of bulk RNA-seq data of mBMDCs treated with synthetic lipid A analogs.

(G) Heatmap of representative ISGs induced by different synthetic lipid A analogs. Shown genes were selected from the DEGs (determined by DEseq2) that are strongly upregulated by 3A-MPLA or 4A-MPLA (total of 556 genes, $\log_2$ [fold change] > 1.0, $p_{adj} < 0.05$). Shown ISGs are highly associated with type I IFNs and IFNAR signaling in immune cells determined by pathway enrichment analysis using Enrichr (76 out of total 556 genes, 13.6%).

n.s., not significant; *$p < 0.05$; **$p < 0.01$; ***$p < 0.001$, unpaired/paired Student's t test. Error bars represent mean ± SEM.

See also Figures S2 and S3 and Tables S3 and S4.

consistent with the sustained type I IFN response that is elicited by 3A- and 4A-MPLA in DCs *in vitro*.

Based on the kinetics of lipid A-induced IFN-β response, we reasoned that lipid A structure may influence its mode of engagement with TLR4, favoring endosomal TLR4 over surface TLR4. Upon LPS or lipid A engagement, monomeric TLR4 is dimerized on the cell surface and then translocated to the early endosome.[27,28] This endocytic process can be assessed by the loss of surface expression of monomeric TLR4 using the monoclonal antibody clone MTS510, which specifically recognizes monomeric but not dimerized TLR4. This decrease in monomeric TLR4 expression upon lipid engagement has been shown to directly correlate with the extent of endocytosed TLR4.[37–39] Using this method, we assessed the degree of TLR4 endocytosis

Please cite this article in press as: Cho et al., Structure of gut microbial glycolipid modulates host inflammatory response, Cell (2025), https://doi.org/10.1016/j.cell.2025.05.016

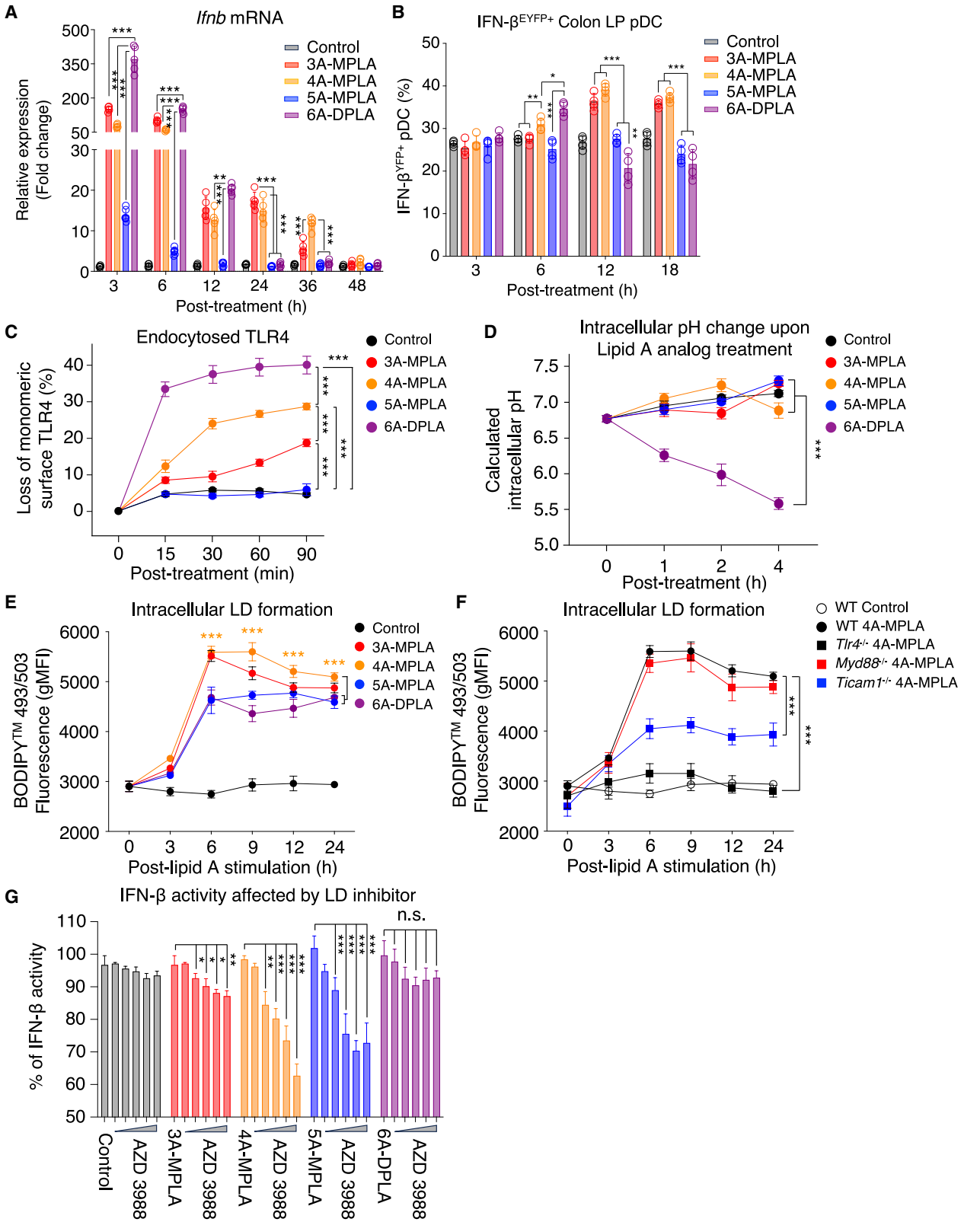

(legend on next page)

Please cite this article in press as: Cho et al., Structure of gut microbial glycolipid modulates host inflammatory response, Cell (2025), https://doi.org/10.1016/j.cell.2025.05.016

modulated by the same set of lipid A analogs examined for their IFN-β response kinetics. 6A-DPLA induced the most rapid and significant reduction in surface expression of monomeric TLR4 at 15 min post stimulation. Among the lipid A analogs reflecting natural lipid A structures found in *Bacteroides* species, 4A-MPLA displayed the most pronounced activity, inducing nearly a 30% reduction in monomeric TLR4 surface expression at 30 min post treatment, whereas 3A-MPLA induced less than a 10% reduction at the same time point (Figure 3C). In contrast, the level of surface TLR4 expression induced by 5A-MPLA was not different from untreated DCs. We also determined changes in TLR4 expression across varying doses of these lipid A analogs and found that their relative potencies were preserved (Figures S5A–S5D).

We next evaluated how lipid A structure influences the efficiency of endocytosis by comparing uptake of fluorescently labeled latex beads coated with different lipid A analogs (Figure S5E). DCs treated with lipid A-coated fluorescent beads displayed a heterogenous pattern of bead uptake, reflected by multiple peaks on the histogram that represent varying levels of endocytosed beads (Figure S5F). We analyzed how the distribution of these peaks (P1–P4) changed depending on the molecular structure of the lipid A analog coating the beads. Compared with other lipid A analogs, beads coated with 4A-MPLA significantly enhanced endocytosis efficiency, increasing the proportion of cells in P4 (more endocytosed beads) while reducing the proportion in P1 (less endocytosed beads). Interestingly, despite its pronounced effect on TLR4 endocytosis, 6A-DPLA failed to exert a comparable level of change on endocytic cargo within P4 relative to 4A-MPLA (Figure S5G).

Following stimulation with LPS or lipid A, endocytosed TLR4 is localized to early endosomes and is subsequently degraded through lysosomal maturation.[27] We hypothesized that the prolonged IFN-β response induced by lipid A analogs is associated with impaired lysosomal maturation following TLR4 engagement. Examination of endosomal maturation using a pH indicator dye revealed that DCs stimulated with 6A-DPLA exhibited a rapid decrease in intracellular pH, consistent with the kinetics of rapid TLR4 endocytosis (Figure 3D). In contrast, none of the MPLA analogs with fewer acyl chains induced such dramatic decreases in intracellular pH. These data strongly suggest that lipid A structure impacts upon lipid A-induced TLR4 endocytosis and endosomal maturation, thereby affecting the sustainability of IFN-β response elicited from the endosome.

Mammalian immune cells accumulate intracellular LDs upon stimulation with various TLR agonists, including bacterial LPS.[40–42] Emerging evidence suggests that IFN-β induces LD accumulation responding to TLR activation, and this LD accumulation corresponds with enhanced/sustained type I IFN production.[43,44] We reasoned that the sustained IFN-β response elicited by 3A- and 4A-MPLA likely correlates with LD accumulation. LD formation in DCs began at 3 h and culminated at 6 h post stimulation (Figure 3E). At the peak of LD formation, both 3A- and 4A-MPLA induced more LD formation compared with 5A-MPLA and 6A-DPLA. Intriguingly, LD formation induced by 3A-MPLA declined by 9 h, whereas the level of LDs induced by 4A-MPLA was more sustained and remained elevated up to 24 h. This pattern of LD formation kinetics in DCs correlates with the prolonged IFN-β response stimulated with 4A-MPLA under both *in vitro* and *in vivo* conditions. Interestingly, the LD formation induced by 4A-MPLA is dependent on TLR4 and TRIF but not MyD88 (Figure 3F), suggesting a close relationship between TLR4-TRIF signaling and LD formation for sustained IFN-β response. Consistently, the IFN-β response induced by 4A-MPLA is susceptible to inhibition by the LD inhibitor AZD 3988, whereas the inhibitory effect of this LD inhibitor on IFN-β production was substantially weaker when DCs were stimulated with other lipid A analogs (Figures 3G, S5H, and S5I).

Cdc42 is the major mediator of endosomal uptake of 4A-MPLA and IFN-β response induced by 4A-MPLA

TLR4 endocytosis triggered by *E. coli*-driven LPS has been known to be dependent on the joint activities of clathrin, dynamin, and Rab proteins.[27,28,31,45] However, how lipid A structure impacts on the mechanism of TLR4-mediated endocytosis has remained elusive. We selected two representative lipid A analogs, 4A-MPLA and 6A-DPLA, which exhibited a contrasting effect on IFN-β response kinetics. With these lipids, we examined lipid A-induced IFN-β response in the presence of various chemical inhibitors targeting distinct regulators of endocytic pathways (Table S5). Consistent with the prior reports, inhibition of endocytic activity by any of these inhibitors resulted in reduced IFN-β production from DCs stimulated with either 4A-MPLA or 6A-DPLA (Figures 4A and 4B). Intriguingly, IFN-β production elicited by 4A-MPLA was markedly reduced by all inhibitors tested, whereas the IFN-β response to 6A-DPLA was comparatively less affected (Figures 4A, 4B, and S6A–S6C). Among the various inhibitors, CASIN, a selective inhibitor targeting Cdc42 GTPase activity, had a limited impact on the IFN-β response induced by 6A-DPLA, in contrast to its marked inhibitory effect on the IFN-β response stimulated with 4A-MPLA (Table S6). However,

Figure 3. IFN-β response to lipid A structure is mediated by the degree of TLR4 endocytosis and LD biogenesis

(A) Kinetics of *Ifnb* mRNA expression in mBMDCs responding to synthetic lipid A analogs.

(B) Proportion of IFN-β-producing plasmacytoid DCs in the colon LP of IFNβ1-EYFP reporter mice in response to a single oral administration of synthetic lipid A analogs (100 μg/mouse).

(C) Percentage loss of monomeric TLR4 expression on the surface after synthetic lipid A analog treatment to mBMDCs at indicated time points.

(D) Changes in intracellular pH of mBMDCs treated with synthetic lipid A analogs. Estimated intracellular pH was calculated by pHrodo Green AM pH indicator dye.

(E and F) Changes in geometric mean fluorescence intensity (gMFI) of BODIPY 493/503 in mBMDCs derived from WT mice and *Tlr4*$^{-/-}$, *Myd88*$^{-/-}$, and *Ticam1*$^{-/-}$ mice after treatment of synthetic lipid A analogs at indicated time points.

(G) Effect of LD inhibitor AZD 3988 (varying dose from 10 to 500 pM) on IFN-β-inducing activity stimulated by different synthetic lipid A analogs.

n.s., not significant; *$p < 0.05$; **$p < 0.01$; ***$p < 0.001$, unpaired/paired Student's t test. Error bars represent mean ± SEM.

See also Figures S4 and S5.

Please cite this article in press as: Cho et al., Structure of gut microbial glycolipid modulates host inflammatory response, Cell (2025), https://doi.org/10.1016/j.cell.2025.05.016

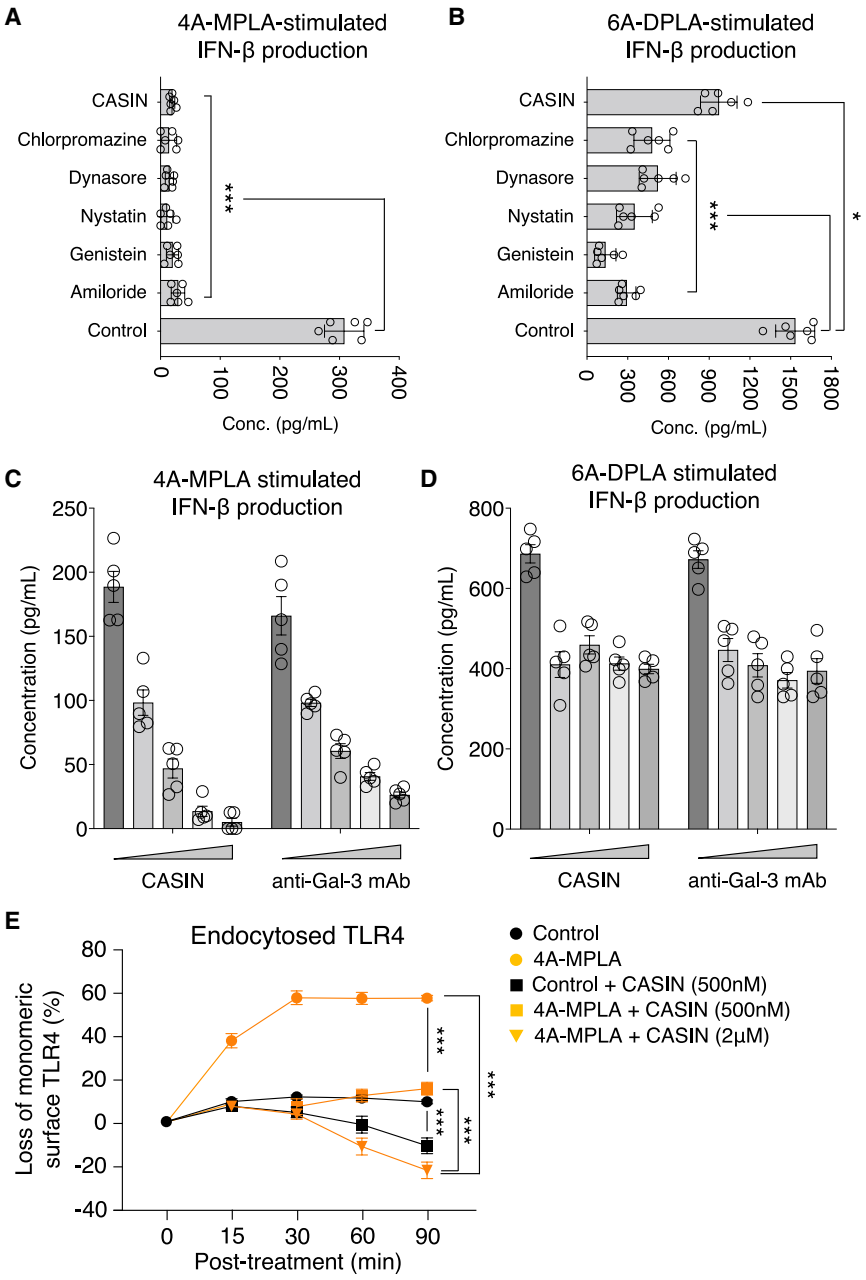

Figure 4. Cdc42 is the major mediator of endosomal uptake of 4A-MPLA and IFN-β response induced by 4A-MPLA

(A and B) Effect of various chemical inhibitors targeting endocytosis on IFN-β response induced by 4A-MPLA (A) or 6A-DPLA (B).

(C and D) Dose effect of Cdc42 inhibitor CASIN (5–1,000 nM) and anti-mouse Gal-3 mAb (0.5–10 μg/mL) on IFN-β response induced by 4A-MPLA (C) or 6A-DPLA (D).

(E) Effect of Cdc42 inhibition using CASIN (500 nM or 2.0 μM) on TLR4 endocytosis in mBMDCs treated with 4A-MPLA.

n.s., not significant; *$p < 0.05$; **$p < 0.01$; ***$p < 0.001$, unpaired/paired Student's t test. Error bars represent mean ± SEM.

See also Figure S6 and Tables S5 and S6.

There was a modest inhibitory effect of 6A-DPLA on IFN-β response exerted by CASIN or anti-mGal-3 mAb, but this impact was limited compared with 4A-MPLA and not dose dependent (Figure 4D). In addition to the inhibitory effect on the IFN-β response, CASIN-mediated Cdc42 inhibition impaired basal TLR4 endocytosis in DCs even in the absence of lipid A stimulation, resulting in a modest increase in surface expression of monomeric TLR4. Upon 4A-MPLA stimulation, Cdc42 inhibition susceptibly reversed the loss of monomeric TLR4 expression, leading to its accumulation on the cell surface (Figure 4E).

CASIN treatment did not inhibit *Il6* mRNA expression in DCs stimulated with either 4A-MPLA or 6A-DPLA (Figure S6D) suggesting a more selective role of Cdc42 activity on the IFN-β response to 4A-MPLA.

Cdc42 is known to regulate clathrin/dynamin-independent endocytosis, and it functions in combination with LPS-binding lectin, galectin-3 (Gal-3).[46–51] To better examine the role of the Cdc42-mediated endocytic process on lipid A-driven IFN-β response, we treated lipid A-stimulated DCs with ranging doses of CASIN or anti-mGal-3 mAb. In response to increasing concentrations of either CASIN or anti-mGal-3, the production of IFN-β induced by 4A-MPLA is proportionally decreased (Figure 4C).

Specific lipid A structure modulates tolerogenic DC function and CD4⁺ T cell responses

Although the less-acylated lipid A analogs elicited more sustained IFN-β responses than 6A-DPLA, the overall magnitude of IFN-β induction remained relatively modest. Consistently, we observed that 3A- and 4A-MPLA analogs induced a group of genes functionally associated with tolerogenic DCs[52–54] (Figure 5A). These less-acylated analogs induced higher expression of coinhibitory molecules compared with 6A-DPLA (Figures 5B and 5C), while simultaneously eliciting lower expression of costimulatory molecules (Figures 5D–5F). Of interest, the LOS purified from *B. fragilis*, which is structurally correlated with these less-acylated lipid A analogs, induced a distinct pattern of both costimulatory and coinhibitory molecule expression compared with *E. coli* LPS.

Next, we examined how lipid A-structure-directed changes in DCs modulate T cell responses associated with tolerogenic DC phenotypes. We added each lipid A analog to DCs co-cultured with naive WT CD4⁺ T cells under various T helper cell (T_H)-polarizing conditions and assessed whether these analogs can inhibit T_H differentiation. Although treatment with lipid A analogs had

Please cite this article in press as: Cho et al., Structure of gut microbial glycolipid modulates host inflammatory response, Cell (2025), https://doi.org/10.1016/j.cell.2025.05.016

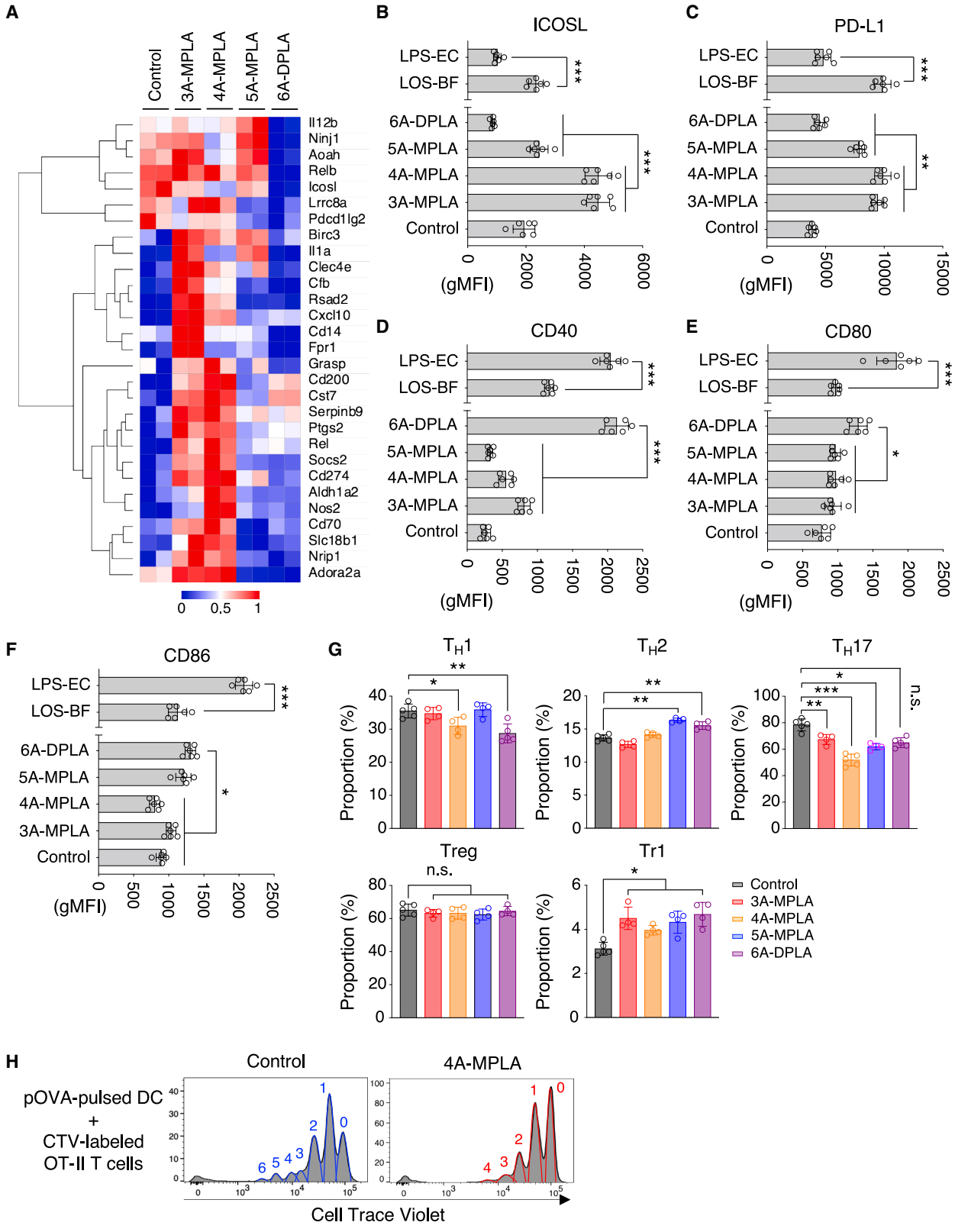

(legend on next page)

Please cite this article in press as: Cho et al., Structure of gut microbial glycolipid modulates host inflammatory response, Cell (2025), https://doi.org/10.1016/j.cell.2025.05.016

minimal effect on the generation of inducible Tregs or Tr1 (Figure 5G, lower), both 4A-MPLA and 6A-DPLA modestly inhibited T_H1 differentiation (Figure 5G, upper left). Of interest, treatment with less-acylated MPLA analogs reduced the proportion of T_H17, with 4A-MPLA showing the most potent inhibitory activity, whereas 6A-DPLA had no noticeable effect (Figure 5G, upper right). Although neither 3A- nor 4A-MPLA showed noticeable activity on T_H2, 5A-MPLA and 6A-DPLA modestly increased the proportion of IL-4-producing cells (Figure 5G, upper middle). These data suggest that the most pronounced immunomodulatory effect induced by these lipid A analogs on T_H response was exerted from 4A-MPLA inhibiting T_H17 differentiation.

We also examined whether 4A-MPLA can exert any effect on antigen-induced T cell proliferation via DCs. In the presence of 4A-MPLA, we pulsed $OVA_{323-339}$ peptides to DCs and then co-cultured them with naive OT-II $CD4^+$ T cells labeled with CellTrace Violet (CTV). Concurrent with its immunomodulatory function on T_H differentiation, the proliferation of CTV-labeled OT-II T cells was markedly impaired in the presence of 4A-MPLA (Figure 5H).

Lipid A-induced IFN-β response regulates induction of RORγt$^+$ Tregs and modulates colonic inflammation

Investigating an underlying mechanism explaining the pronounced impact of 4A-MPLA on colitis, we examined whether this effect was still present in the absence of T cells and/or innate lymphoid cells. Pre-treatment with 4A-MPLA in *Rag1*$^{-/-}$ *Il2rg*$^{-/-}$ or *Tcrb*$^{-/-}$ mice prior to the induction of colitis confirmed that the 4A-MPLA-driven protective response was abolished (Figures S7A and S7B). This indicates that T cells are required for 4A-MPLA-driven immunomodulation to control colonic inflammation.

Modulation of colonic Tregs is central to maintaining intestinal immune homeostasis. The RORγt$^+$ Treg subset lacking Helios (thymically derived Treg marker)[55] represents a peripherally induced Treg that is functionally superior in controlling colonic inflammation compared with its RORγt$^-$ Treg counterparts[56,57] and is highly influenced by gut microbiota.[16,18] Although we did not find any noticeable impact of lipid A synthetic analogs on the overall colonic Treg proportion (Figure 6A, left), the frequency of RORγt$^+$ Tregs was meaningfully increased in response to 4A-MPLA (and, to a lesser extent, by 3A-MPLA) treatment at day 7 (Figure 6A, right). In contrast, the frequency of RORγt$^+$ colonic Tregs was significantly decreased when either 5A-MPLA or 6A-DPLA was administered to the mice prior to DSS challenge. In addition, we also examined the impact of lipid A structure on colonic RORγt$^+$ Tregs at the steady-state condition via the oral administration of each lipid A analog to germ-free (GF) and specific pathogen-free (SPF) WT mice. In both conditions, the administration of 4A-MPLA upregulated RORγt$^+$ Tregs in the colon, while 3A-MPLA contributed to only a marginal increase in these cells during colonic inflammation (Figures S7C and S7D). Also, 5A-MPLA and 6A-DPLA had opposing effects on colonic RORγt$^+$ Tregs in SPF mice, although this was not observed under the GF condition. These results indicate that 4A-MPLA exerts a similar function on colonic Tregs during homeostasis, regardless of the presence of gut microbiota. Of interest, the increase in RORγt$^+$ colonic Tregs by 4A-MPLA treatment is associated with their functional phenotype producing more IL-10 at day 7 of DSS-induced colitis (Figures S7E and S7F). The ablation of RORγt$^+$ Tregs (*Rorc*$^{\Delta Treg}$) exacerbated the severity of DSS-induced colitis in mice (Figure 6B) as previously reported,[18] and we observed a similar phenotype with a spontaneous increase in IL-17-producing colonic $CD4^+$ T cells without any treatment (Figure 6C). Of note, the oral administration of 4A-MPLA or any other lipid A analogs did not elicit a protective response in the Rorc$^{\Delta Treg}$ mice, highlighting the importance of RORγt$^+$ Tregs during colonic inflammation.

The functional impact of type I IFN signaling on Tregs has been previously studied.[58–60] However, there has not been a detailed mechanistic evaluation of this functional impairment in *Ifnar1*$^{-/-}$ Tregs, and the role of type I IFN signaling in the RORγt$^+$ colonic Treg subset has received little attention. Owing to the substantial IFN-β activity induced by 4A-MPLA, we examined the impact of IFN-β-mediated signaling on the immunomodulatory effect exerted by 4A-MPLA during colonic inflammation. Of interest, *Ifnar1*$^{-/-}$ mice receiving 4A-MPLA failed to elicit the immunoprotective effect on IL-17A and IFN-γ production by colonic $CD4^+$ T cells (Figures 6D and 6E). Analysis of colonic Tregs in naive *Ifnar1*$^{-/-}$ mice revealed a close functional relationship between type I IFN signaling and RORγt expression in Tregs. Although total Treg cell frequency remained unchanged, the proportion of RORγt$^+$ colonic Tregs was significantly reduced. Of interest, this change coincided with a marked increase of T_H17-phenotpe (RORγt$^+$) cells in the colon among conventional $CD4^+$ T cells (T_{conv}), which do not express Foxp3 (Figure 6F). When *Ifnar1* deficiency is limited to Foxp3$^+$ cells (*Ifanr1*$^{\Delta Treg}$), 4A-MPLA could no longer elicit a protective response in *Ifanr1*$^{\Delta foxp3}$ mice challenged with DSS and failed to control IL-17A and IFN-γ production from colitogenic $CD4^+$ T cells, as observed in *Ifanr1*$^{-/-}$ mice (Figures S7G and S7H). Additionally, IL-17A production was elevated in *Ifanr1*$^{\Delta Treg}$ mice compared with those with intact IFNAR1 (*Ifanr1*^{WT}), whereas IFN-γ-producing cells remained unaffected at day 7 of DSS-induced colitis. We also confirmed the observation that *Ifanr1*$^{\Delta Treg}$ mice phenocopy the status of colonic Tregs in *Ifnar1*$^{-/-}$ mice by having reduced RORγt expression within colonic Tregs without any change in overall Treg cell

Figure 5. Specific lipid A structure modulates tolerogenic DC function and $CD4^+$ T cell responses

(A) Heatmap of genes functionally associated with tolerogenic dendritic cells in response to stimulation of lipid A analogs from mBMDCs.

(B–F) Surface expression of representative DC phenotype markers, ICOSL (B), PD-L1 (C), CD40 (D), CD80 (E), and CD86 (F) in response to stimulation by different synthetic lipid A analogs from mBMDCs.

(G) Effects of synthetic lipid A analogs on differentiation of $CD4^+$ helper T cells (T_H1, T_H2, T_H17, Treg, and Tr1) under each individual polarizing condition in DC-T cell co-cultures. Proportions of IFN-γ$^+$ (T_H1), IL-4$^+$ (T_H2), IL-17A$^+$ (T_H17), Foxp3$^+$ (Treg), and IL-10$^+$ (Tr1) among the cultured $CD4^+$ T cells are shown.

(H) Effect of 4A-MPLA on the proliferation of Ag-induced OT-II TCR T cells labeled with CTV dye in the presence of OVA-pulsed DCs.

n.s., not significant; *$p < 0.05$; **$p < 0.01$; ***$p < 0.001$, unpaired/paired Student's t test. Error bars represent mean ± SEM.

Please cite this article in press as: Cho et al., Structure of gut microbial glycolipid modulates host inflammatory response, Cell (2025), https://doi.org/10.1016/j.cell.2025.05.016

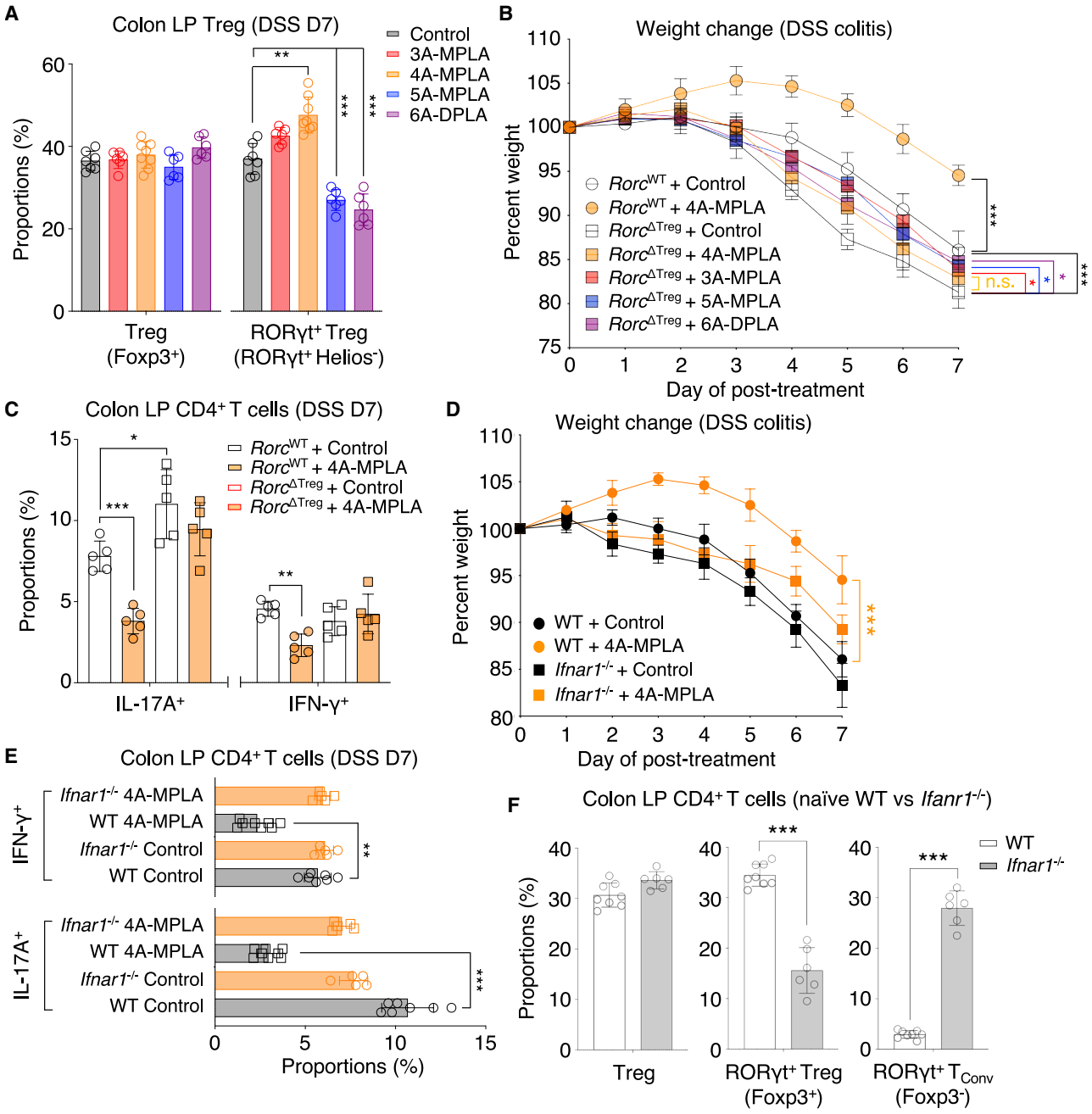

Figure 6. Lipid A-induced IFN-β response regulates induction of RORγt$^+$ Tregs and modulates colonic inflammation

(A) Proportion of colonic LP Tregs (Foxp3$^+$) and RORγt$^+$ Tregs (RORγt$^+$ Helios$^-$) within Tregs at day 7 post DSS treatment (DSS day 7).

(B and C) Immunoprotective effect of 4A-MPLA and other lipid A analogs on DSS-induced colitis in *Foxp3-cre* × *Rorc*$^{+/+}$ (*Rorc*^{WT}) or *Rorc*$^{f/f}$ (*Rorc*$^{\Delta Treg}$) determined by weight changes during DSS treatment (B) and colitogenic cytokine productions (IL-17A and IFN-γ) from colon LP CD4$^+$ T cells at day 7 post DSS treatment (DSS day 7) (C).

(D and E) Effect of IFN-β-mediated signaling on immunoprotective response induced by 4A-MPLA treatment in DSS-induced colitis model in *Ifnar1*$^{-/-}$ mice. Weight change (D) and cytokine production (IL-17A and IFN-γ) from colon LP CD4$^+$ T cells at DSS day 7 (E) are shown.

(F) Proportion of colon LP Tregs (Foxp3$^+$) among CD4$^+$ T cells (left), RORγt$^+$ Tregs (RORγt$^+$ Helios$^-$) within Treg subset (middle), and RORγt$^+$ (T_H17-phenotype) conventional CD4$^+$ T cells (T_{Conv}) among Foxp3$^-$ CD4$^+$ T cells from naive WT vs. *Ifnar1*$^{-/-}$ mice (right).

n.s., not significant; *$p < 0.05$; **$p < 0.01$; ***$p < 0.001$, unpaired/paired Student's t test. Error bars represent mean ± SEM.

See also Figure S7.

Please cite this article in press as: Cho et al., Structure of gut microbial glycolipid modulates host inflammatory response, Cell (2025), https://doi.org/10.1016/j.cell.2025.05.016

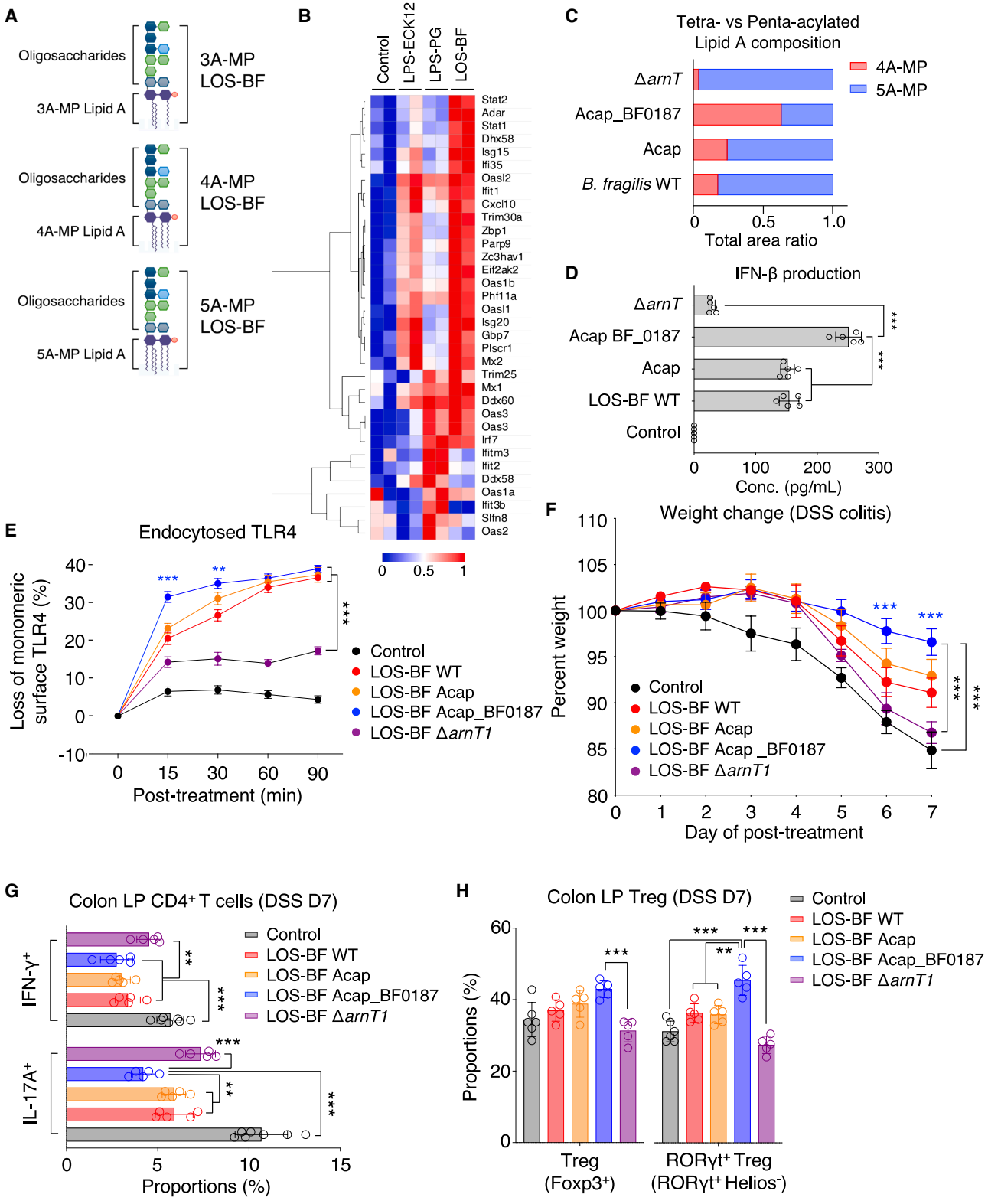

Figure 7. The natural lipid A in *Bacteroides* LOS and synthetic lipid A have similar immunobiology

(A) Schematic diagram of LOS (lipid A with attached oligosaccharides) from *B. fragilis* (LOS-BF) containing lipid A species with tri-, tetra-, and penta-acyl chains with a single phosphate group (3A- to 5A-MP).

(legend continued on next page)

Please cite this article in press as: Cho et al., Structure of gut microbial glycolipid modulates host inflammatory response, Cell (2025), https://doi.org/10.1016/j.cell.2025.05.016

frequency in the steady-state condition (*Ifanr1*$^{\Delta Treg}$ no DSS). At the peak of DSS-induced colonic inflammation, the impaired RORγt$^+$ colonic Tregs from *Ifanr1*$^{\Delta Treg}$ mice were not restored by 4A-MPLA treatment when IFNAR1 was absent (*Ifanr1*$^{\Delta Treg}$ + 4A-MPLA, DSS day 7). Although 4A-MPLA treatment enhanced the RORγt$^+$ Treg subset from *Ifanr1*^{WT} mice, as observed in WT mice with DSS challenge, we still could not find a notable change in overall colonic Treg frequency at day 7 of colitis (*Ifanr1*^{WT} + 4A-MPLA, DSS day 7) (Figure S7I).

Recent studies have shown that major histocompatibility complex (MHC)II-expressing RORγt$^+$ antigen-presenting cell (APC) ("Thetis" cells or "Janus" cells) plays an important role in the generation of colonic RORγt$^+$ Tregs.[61–63] We sought to determine the impact of lipid A on IFN-β induction of this subset using IFNβ1-EYFP reporter mice. Upon administration of lipid A analogs, this RORγt$^+$ APC subset produced IFN-β, although the induction of IFN-β was less prominent in this subset compared with other colonic APCs (cDC1/2 plus pDC) examined (Figure S7J). Collectively, these data indicate that the structure of lipid A impacts on the colonic Tregs by enhancing RORγt expression, promoting their effector function to better control gut inflammation. In this process, type I IFN signaling via IFNAR1 reinforces Tregs suppression and maintains Treg-T_H17 balance during homeostasis.

The natural lipid A in *Bacteroides* LOS and synthetic lipid A have similar immunobiology

We observed a strong upregulation of type I IFN-responsive genes in DCs treated with LOS (a mixture of 3A- to 5A-MP lipid A) isolated from *B. fragilis* (Figure 7A), in contrast to the ISG signature induced by LPS isolated from *P. gingivalis* or *E. coli* (Figure 7B). Notably, *P. gingivalis* LPS predominantly contains penta-acylated lipid A, whereas *E. coli* lipid A is entirely hexa-acylated.[64] As previously reported,[33] the composition of lipid A structures across Bacteroidetes are overall relatively similar to that of *B. fragilis* (Figure S7K). Supporting this notion, LOS isolated from different *Bacteroides* species share a common ability to induce IFN-β with only modest differences in their potency (Figure S7L). We hypothesized that the immunological effects governed by structural attributes of synthetic lipid A analogs can also be recapitulated by natural lipid A of *Bacteroides*. To test this, we used a mutant strain of *B. fragilis* that does not produce capsular polysaccharides (*Acap*)[65] to increase the yield of LOS. Using this strain, we induced the expression of lipid A deacetylase gene (*Acap_BF0187*)[66] to enhance the production of tetra-acylated lipid A species. We also knocked out the *arnT* gene[67] in another mutant, resulting in a biased penta-acylated lipid A phenotype (Figure 7C; Table S7). We purified the LOS from these *B. fragilis* mutants and confirmed that each mutant exhibits different natural lipid A ratios of 4A-MP and 5A-MP. Although both WT and *Acap* mutant exhibited similar natural 4A-MP/5A-MP lipid A ratios, the *Acap_BF0187* mutant exhibited a 4-fold increase in 4A-MP and a 2-fold decrease in 5A-MP compared with WT and *Acap* mutant. The *ΔarnT* mutant displayed a 6-fold decrease in 4A-MP with a 2.5-fold increase in 5A-MP compared with the levels in the *Acap_BF0187* mutant. The 4A-MP-enriched LOS (*Acap_BF0187*) induced higher IFN-β response than was induced by the LOS purified from either WT or *Acap* mutant. Consistent with our results on 5A-MPLA, the 5A-MP-biased LOS (*ΔarnT*) showed significantly impaired IFN-β response (Figure 7D). Consistent with these data, the *Acap_BF0187* LOS induced TLR4 endocytosis more efficiently at earlier time points (15 and 30 min) compared with the LOS from WT and *Acap* (Figure 7E). As expected, the *ΔarnT* LOS induced relatively minimal levels of TLR4 endocytosis compared with the LOS isolated from WT and other mutants.

To examine whether structural modifications of natural lipid A induce *in vivo* responses similar to those elicited by lipid A analogs, we orally administered the LOS from *B. fragilis* WT and mutants to mice prior to DSS treatment. The LOS purified from WT and all mutants elicited immunoprotective responses distinguishable from the untreated control group by day 3. Notably, mice treated with *Acap_BF0187* LOS exhibited less weight loss and reduced IL-17A production by colitogenic CD4$^+$ T cells compared with those treated with LOS isolated from WT and other mutants. The weak activity in inducing IFN-β and TLR4 endocytosis observed with 5A-MPLA was similarly seen with *ΔarnT* LOS, which conferred reduced protection compared with *Acap_BF0187* (Figure 7F). Interestingly, while *Acap_BF0187* LOS treatment increased the proportion of colonic RORγt$^+$ Tregs, *ΔarnT* LOS resulted in a markedly lower RORγt$^+$ Treg proportion (Figure 7G). We also examined the activity of various *Bacteroides* LOS on RORγt$^+$ Tregs under *in vitro* RORγt$^+$ Treg-inducing condition. Under this condition, *Bacteroides* LOS increased the RORγt$^+$ Treg proportion, whereas 6A-DPLA attenuated this activity

(B) Heatmap of representative ISGs (the same set shown in Figure 2G) induced by different bacterial glycolipid extracts (LPS-ECK12, LPS isolated from *Escherichia coli* K-12; LPS-PG, LPS isolated from *Porphyromonas gingivalis*; LOS-BF, LOS isolated from *B. fragilis* NCTC 9343).
(C) Ratio of tetra-acylated (4A-MP) vs. penta-acylated monophosphoryl (5A-MP) lipid A species present in *B. fragilis* WT and lipid A mutant strains. Shown ratios are calculated from the total area in total ion chromatogram of LC-MS compiled from multiple cultured batches. Shown lipid A species are found in the LOS purified from *B. fragilis* WT, *B. fragilis* acapsular mutant (Acap), *B. fragilis* Acap mutant inducibly expressing BF0187 (Acap_BF0187), and *B. fragilis* mutant lacking 4-amino-4-deoxy-L-arabinose transferase (*ΔarnT*).
(D) IFN-β response from mBMDCs stimulated with purified LOS (1.0 μg/mL) from *B. fragilis* WT and other lipid A mutant strains.
(E) Percentage loss of monomeric TLR4 expression on the surface of mBMDCs after treatment of *B. fragilis* LOS harvested from WT and other lipid A mutant strains at indicated time points.
(F–H) Immunoprotective effect of oral administration of *B. fragilis* LOS purified from WT and other lipid A mutant strains on DSS-induced colonic inflammation, as determined by weight changes during DSS treatment (F), colitogenic cytokine production (IL-17A and IFN-γ) from colon LP CD4$^+$ T cells (G), and Tregs (Foxp3$^+$) and RORγt expression within Tregs (H) at day 7 post DSS treatment (DSS day 7).
n.s., not significant; $^*p < 0.05$; $^{**}p < 0.01$; $^{***}p < 0.001$, unpaired/paired Student's t test. Error bars represent mean ± SEM.
See also Figure S7 and Table S7.

Please cite this article in press as: Cho et al., Structure of gut microbial glycolipid modulates host inflammatory response, Cell (2025), https://doi.org/10.1016/j.cell.2025.05.016

(Figure S7M). Collectively, these data demonstrate that structural changes in natural symbiotic lipid A mimic the functional effects observed with synthetic lipid A analogs. These effects are mediated through IFN-β on Tregs both *in vitro* and *in vivo*, highlighting the importance of endobiotic balance in lipid A structure and revealing a potential risk for dysbiosis.

DISCUSSION

Our lipidomic profiling revealed *B. fragilis* lipid A exists in multiple forms, varying in acyl chain numbers and having a single phosphate group. To develop mechanistic insight into these structurally diverse lipid As, we used chemically synthesized lipid A analogs corresponding to the natural lipid A structure found in Bacteroidetes. Our transcriptomic analysis of DCs stimulated with these analogs revealed a gene expression module responsive to specific molecular patterns in lipid A functionally associated with type I IFNs and ISGs. These lipid A analogs displayed varying binding affinities to the TLR4-MD2 and induced different degrees of TLR4 endocytosis, which functionally correlated with IFN-β production. Genetic modification of *B. fragilis* lipid A structures resulted in LOS that induced immunological effects similar to those elicited by synthetic lipid A analogs, despite accompanying structural changes in lipid A (e.g., the removal of hexuronic acid in *ΔarnT* mutant).[67] Considering the structural commonality of lipid A across the Bacteroidetes phylum, our study demonstrates the importance of endobiotic balance in these symbiont lipid A structures.

Previous studies suggest a possible functional role of type I IFN signaling in Tregs. IFNAR1-deficient Tregs failed to control autoimmune inflammation.[59,68,69] Although a correlation between colonic RORγt$^+$ Tregs and microbiota via TLR4 signaling has been reported,[70] it is still unknown which microbial molecules and mechanisms regulate RORγt$^+$ Treg homeostasis. We find a functional link between lipid A and colonic RORγt$^+$ Tregs, tightly associated with IFNAR signaling. Importantly, the ablation of IFNAR either globally or specifically in the Treg lineage significantly reduces colonic RORγt$^+$ Treg proportion and leads to a spontaneous increase in colonic T_H17 cells under steady-state conditions. Collectively, we find a functional role of commensal lipid A-induced IFN-β signaling on colonic RORγt$^+$ Treg homeostasis. As previously reported, deletion of IFNAR results in T_H17 dysregulation,[71–73] and our results indicate that this may be partly due to a failure in RORγt$^+$ Treg homeostasis, which is critical for peripheral tolerance, preventing spontaneous T_H17 activation in the intestine.

Recent studies have reported a pivotal role of RORγt$^+$ APC subset for the development of colonic RORγt$^+$ Tregs.[61–63] The central function of this subset on RORγt$^+$ Tregs is to present an antigen on their MHCII, but the identity of this antigen remains elusive. Although it is unlikely that lipid A is directly presented on MHCII by this RORγt$^+$ APC subset, we noticed that it similarly modulated IFN-β induction in RORγt$^+$ APC and other DCs subsets. However, under steady-state conditions, the proportion of IFN-β-producing cells within RORγt$^+$ APCs was lower than observed in colonic pDCs. The similar IFN-β response pattern between colonic RORγt$^+$ APC and pDC to lipid A structures suggests that IFN-β response in these cells is likely regulated by TLR4. Although IFN-β induction in response to lipid A is more prominent in colonic pDC compared with other cDC subsets, we observed strong induction of ISGs in cultured mBMDC *in vitro*, which consist primarily of immature cDCs. Although further studies are warranted to examine this discrepancy, colonic pDCs appear more responsive to microbiota-driven cues in their ability to induce IFN-β, whereas this capacity remains largely unaltered in cDCs. These results suggest that colonic pDCs may have an enhanced ability to sense changes in lipid A structure and to induce immunomodulatory responses associated with type I IFNs.

Molecular inhibitors targeting clathrin and/or dynamin have been reported to control LPS-induced TLR4 endocytosis.[27,31,39] Consistently, 6A-DPLA-stimulated IFN-β induction was effectively inhibited by the chemical inhibitors targeting clathrin-mediated pathway or dynamin GTPase. However, neither Cdc42 inhibition nor Gal-3 neutralization effectively inhibited IFN-β responses induced by 6A-DPLA. In contrast, the IFN-β induced by 4A-MPLA was readily inhibited by either a Cdc42 inhibitor or anti-Gal-3 mAb. These results suggest that the chemical structure of lipid A dictates the mechanism of TLR4 endocytosis. Of note, Cdc42 is also one of the downstream genes activated by IFN-β.[74–76] Although further studies are needed to understand how Cdc42 is being selected upon TLR4 interaction with a specific structure of lipid A, it is plausible that there is a positive feedback loop activated by a sustained type I IFN response elicited by a TLR4 agonist such as 4A-MPLA.

Emerging evidence suggests that LDs play an important role in type I IFN responses. Upon LPS stimulation, LDs are being accumulated inside the cell, and this functions as a signaling platform by expressing various type I IFN-inducible proteins on their surface.[41,77] Of interest, the accumulated LDs amplify type I IFN responses and upregulate ISG expression enhancing the anti-viral state of immune cells.[43,44] Among the lipid A analogs tested, 4A-MPLA exhibited the most pronounced activity to induce and sustain LD formation. Given the positive feedback between LD and IFN-β response, along with the susceptibility of this response to LD inhibition, our findings suggest that the sustained IFN-β response induced by 4A-MPLA is closely linked to TRIF-dependent LD formation through endosomal TLR4 signaling. This highlights a previously underappreciated link between lipid A structure and LD-mediated immune regulation of innate immune response.

We have uncovered previously unexplored relationships between symbiotic lipid A structures and immunomodulatory activities, illustrating a functional correlation between commensal lipid A molecular structure and a specific immunological activity modulating a peripheral Treg subset in the colon. Our findings strongly indicate that, among the various synthetic and biogenic lipid A structures, 4A-MPLA is the most potent inducer of a protective IFN-β-mediated immunomodulatory response that mitigates colonic inflammation. Insights gained into the functional pathways of these lipids will enable further definition of structural features critical for optimizing specific immune responses.

Limitations of the study

Among the theoretically possible structural attributes, we focused on the number of acyl chains and the impact of a single

phosphate group. Obviously, many other chemical features could possibly be examined. We reasoned that the biggest impact on immune response in naturally occurring lipid A from symbionts would be appreciated by examining these two variables. Further structure-function work on these molecules will necessitate extensive input from synthetic chemistry. Although we examined the impact of lipid A structure on the binding affinity with the TLR4-MD2 complex, future structural studies are warranted to investigate the underlying mechanism of molecular interaction between this complex and symbiotic lipid A molecules and to understand how these interactions are distinguishable from the interaction with the conventional LPS or lipid A structure.

RESOURCE AVAILABILITY

Lead contact

Further information and any requests for experimental resources and reagents used in this study should be directed to, and will be fulfilled by, the lead contact, Dennis L. Kasper (dennis_kasper@hms.harvard.edu).

Materials availability

Bacterial mutant strains and synthesized lipid A analogs generated for this study will be available upon request.

Data and code availability

Bulk RNA-seq data have been submitted to the Gene Expression Omnibus repository (GEO: GSE296696). All codes used for this study are available on GitHub.

ACKNOWLEDGMENTS

We thank HMS BPF and Flow Core for their assistance. We thank Jun Huh, Ruaidhri Jackson, Stefanie Schmieder, and Wayne Lencer for their feedback on the manuscript. This work was supported by a Research Fellows Award from Crohn's and Colitis Foundation (649279 to H.-S.C.), the Department of Defense, United States (W81XWH1910625 and HT94252310226 to D.L.K.; W81XWH1910626 to S.F.O.), and National Institutes of Health, United States (R01AT010268 to S.F.O.).

AUTHOR CONTRIBUTIONS

Conceptualization, H.-S.C. and D.L.K.; methodology, H.-S.C. and X.S.; formal analysis, A.D., B.G., and S.F.O.; investigation, H.-S.C.; resources, J.-S.Y., J.L., S.S., and Y.S.H.; writing—original draft, H.-S.C.; writing—review, S.F.O., S.B.P., and D.L.K.; visualization, H.-S.C.; supervising co-senior authors, S.F.O., S.B.P., and D.L.K.; and funding acquisition, H.-S.C., S.F.O., and D.L.K.

DECLARATION OF INTERESTS

A patent application has been filed by Harvard University based on the work reported in this manuscript.

STAR★METHODS

Detailed methods are provided in the online version of this paper and include the following:

SUPPLEMENTAL INFORMATION

Supplemental information can be found online at https://doi.org/10.1016/j.cell.2025.05.016.

Received: October 9, 2024
Revised: February 27, 2025
Accepted: May 16, 2025

REFERENCES

1. Kamada, N., Seo, S.U., Chen, G.Y., and Núñez, G. (2013). Role of the gut microbiota in immunity and inflammatory disease. Nat. Rev. Immunol. *13*, 321–335. https://doi.org/10.1038/nri3430.
2. Belkaid, Y., and Hand, T.W. (2014). Role of the microbiota in immunity and inflammation. Cell *157*, 121–141. https://doi.org/10.1016/j.cell.2014.03.011.
3. Nicholson, J.K., Holmes, E., Kinross, J., Burcelin, R., Gibson, G., Jia, W., and Pettersson, S. (2012). Host-gut microbiota metabolic interactions. Science *336*, 1262–1267. https://doi.org/10.1126/science.1223813.
4. Rooks, M.G., and Garrett, W.S. (2016). Gut microbiota, metabolites and host immunity. Nat. Rev. Immunol. *16*, 341–352. https://doi.org/10.1038/nri.2016.42.
5. Michaudel, C., and Sokol, H. (2020). The Gut Microbiota at the Service of Immunometabolism. Cell Metab. *32*, 514–523. https://doi.org/10.1016/j.cmet.2020.09.004.
6. Zheng, W., Zhao, W., Wu, M., Song, X., Caro, F., Sun, X., Gazzaniga, F., Stefanetti, G., Oh, S., Mekalanos, J.J., et al. (2020). Microbiota-targeted maternal antibodies protect neonates from enteric infection. Nature *577*, 543–548. https://doi.org/10.1038/s41586-019-1898-4.
7. Stefan, K.L., Kim, M.V., Iwasaki, A., and Kasper, D.L. (2020). Commensal Microbiota Modulation of Natural Resistance to Virus Infection. Cell *183*, 1312–1324.e10. https://doi.org/10.1016/j.cell.2020.10.047.
8. Abt, M.C., Osborne, L.C., Monticelli, L.A., Doering, T.A., Alenghat, T., Sonnenberg, G.F., Paley, M.A., Antenus, M., Williams, K.L., Erikson, J., et al. (2012). Commensal bacteria calibrate the activation threshold of innate antiviral immunity. Immunity *37*, 158–170. https://doi.org/10.1016/j.immuni.2012.04.011.
9. Mazmanian, S.K., Liu, C.H., Tzianabos, A.O., and Kasper, D.L. (2005). An immunomodulatory molecule of symbiotic bacteria directs maturation of the host immune system. Cell *122*, 107–118. https://doi.org/10.1016/j.cell.2005.05.007.
10. Mazmanian, S.K., Round, J.L., and Kasper, D.L. (2008). A microbial symbiosis factor prevents intestinal inflammatory disease. Nature *453*, 620–625. https://doi.org/10.1038/nature07008.

11. Dasgupta, S., Erturk-Hasdemir, D., Ochoa-Reparaz, J., Reinecker, H.C., and Kasper, D.L. (2014). Plasmacytoid dendritic cells mediate anti-inflammatory responses to a gut commensal molecule via both innate and adaptive mechanisms. Cell Host Microbe *15*, 413–423. https://doi.org/10.1016/j.chom.2014.03.006.

12. Ochoa-Repáraz, J., Mielcarz, D.W., Ditrio, L.E., Burroughs, A.R., Begum-Haque, S., Dasgupta, S., Kasper, D.L., and Kasper, L.H. (2010). Central nervous system demyelinating disease protection by the human commensal Bacteroides fragilis depends on polysaccharide A expression. J. Immunol. *185*, 4101–4108. https://doi.org/10.4049/jimmunol.1001443.

13. Ochoa-Repáraz, J., Mielcarz, D.W., Wang, Y., Begum-Haque, S., Dasgupta, S., Kasper, D.L., and Kasper, L.H. (2010). A polysaccharide from the human commensal Bacteroides fragilis protects against CNS demyelinating disease. Mucosal Immunol. *3*, 487–495. https://doi.org/10.1038/mi.2010.29.

14. Bäumler, A.J., and Sperandio, V. (2016). Interactions between the microbiota and pathogenic bacteria in the gut. Nature *535*, 85–93. https://doi.org/10.1038/nature18849.

15. Blander, J.M., Longman, R.S., Iliev, I.D., Sonnenberg, G.F., and Artis, D. (2017). Regulation of inflammation by microbiota interactions with the host. Nat. Immunol. *18*, 851–860. https://doi.org/10.1038/ni.3780.

16. Song, X., Sun, X., Oh, S.F., Wu, M., Zhang, Y., Zheng, W., Geva-Zatorsky, N., Jupp, R., Mathis, D., Benoist, C., et al. (2020). Microbial bile acid metabolites modulate gut RORgamma(+) regulatory T cell homeostasis. Nature *577*, 410–415. https://doi.org/10.1038/s41586-019-1865-0.

17. Geva-Zatorsky, N., Sefik, E., Kua, L., Pasman, L., Tan, T.G., Ortiz-Lopez, A., Yanortsang, T.B., Yang, L., Jupp, R., Mathis, D., et al. (2017). Mining the Human Gut Microbiota for Immunomodulatory Organisms. Cell *168*, 928–943.e11. https://doi.org/10.1016/j.cell.2017.01.022.

18. Sefik, E., Geva-Zatorsky, N., Oh, S., Konnikova, L., Zemmour, D., McGuire, A.M., Burzyn, D., Ortiz-Lopez, A., Lobera, M., Yang, J., et al. (2015). MUCOSAL IMMUNOLOGY. Individual intestinal symbionts induce a distinct population of RORgamma(+) regulatory T cells. Science *349*, 993–997. https://doi.org/10.1126/science.aaa9420.

19. Galanos, C., Lüderitz, O., Rietschel, E.T., Westphal, O., Brade, H., Brade, L., Freudenberg, M., Schade, U., Imoto, M., and Yoshimura, H. (1985). Synthetic and natural Escherichia coli free lipid A express identical endotoxic activities. Eur. J. Biochem. *148*, 1–5. https://doi.org/10.1111/j.1432-1033.1985.tb08798.x.

20. Molinaro, A., Holst, O., Di Lorenzo, F., Callaghan, M., Nurisso, A., D'Errico, G., Zamyatina, A., Peri, F., Berisio, R., Jerala, R., et al. (2015). Chemistry of lipid A: at the heart of innate immunity. Chemistry *21*, 500–519. https://doi.org/10.1002/chem.201403923.

21. Zafar, H., and Saier, M.H., Jr. (2021). Gut Bacteroides species in health and disease. Gut Microbes *13*, 1–20. https://doi.org/10.1080/19490976.2020.1848158.

22. Vatanen, T., Kostic, A.D., d'Hennezel, E., Siljander, H., Franzosa, E.A., Yassour, M., Kolde, R., Vlamakis, H., Arthur, T.D., Hämäläinen, A.M., et al. (2016). Variation in Microbiome LPS Immunogenicity Contributes to Autoimmunity in Humans. Cell *165*, 1551. https://doi.org/10.1016/j.cell.2016.05.056.

23. Erturk-Hasdemir, D., Oh, S.F., Okan, N.A., Stefanetti, G., Gazzaniga, F.S., Seeberger, P.H., Plevy, S.E., and Kasper, D.L. (2019). Symbionts exploit complex signaling to educate the immune system. Proc. Natl. Acad. Sci. USA *116*, 26157–26166. https://doi.org/10.1073/pnas.1915978116.

24. Duan, T., Du, Y., Xing, C., Wang, H.Y., and Wang, R.F. (2022). Toll-Like Receptor Signaling and Its Role in Cell-Mediated Immunity. Front. Immunol. *13*, 812774. https://doi.org/10.3389/fimmu.2022.812774.

25. Gangloff, M. (2012). Different dimerisation mode for TLR4 upon endosomal acidification? Trends Biochem. Sci. *37*, 92–98. https://doi.org/10.1016/j.tibs.2011.11.003.

26. Watts, C. (2008). Location, location, location: identifying the neighborhoods of LPS signaling. Nat. Immunol. *9*, 343–345. https://doi.org/10.1038/ni0408-343.

27. Husebye, H., Halaas, Ø., Stenmark, H., Tunheim, G., Sandanger, Ø., Bogen, B., Brech, A., Latz, E., and Espevik, T. (2006). Endocytic pathways regulate Toll-like receptor 4 signaling and link innate and adaptive immunity. EMBO J. *25*, 683–692. https://doi.org/10.1038/sj.emboj.7600991.

28. Husebye, H., Aune, M.H., Stenvik, J., Samstad, E., Skjeldal, F., Halaas, O., Nilsen, N.J., Stenmark, H., Latz, E., Lien, E., et al. (2010). The Rab11a GTPase controls Toll-like receptor 4-induced activation of interferon regulatory factor-3 on phagosomes. Immunity *33*, 583–596. https://doi.org/10.1016/j.immuni.2010.09.010.

29. Kagan, J.C., and Medzhitov, R. (2006). Phosphoinositide-mediated adaptor recruitment controls Toll-like receptor signaling. Cell *125*, 943–955. https://doi.org/10.1016/j.cell.2006.03.047.

30. Medzhitov, R., Preston-Hurlburt, P., Kopp, E., Stadlen, A., Chen, C., Ghosh, S., and Janeway, C.A., Jr. (1998). MyD88 is an adaptor protein in the hToll/IL-1 receptor family signaling pathways. Mol. Cell *2*, 253–258. https://doi.org/10.1016/s1097-2765(00)80136-7.

31. Kagan, J.C., Su, T., Horng, T., Chow, A., Akira, S., and Medzhitov, R. (2008). TRAM couples endocytosis of Toll-like receptor 4 to the induction of interferon-beta. Nat. Immunol. *9*, 361–368. https://doi.org/10.1038/ni1569.

32. Brubaker, S.W., Bonham, K.S., Zanoni, I., and Kagan, J.C. (2015). Innate immune pattern recognition: a cell biological perspective. Annu. Rev. Immunol. *33*, 257–290. https://doi.org/10.1146/annurev-immunol-032414-112240.

33. d'Hennezel, E., Abubucker, S., Murphy, L.O., and Cullen, T.W. (2017). Total Lipopolysaccharide from the Human Gut Microbiome Silences Toll-Like Receptor Signaling. mSystems *2*. e00046–17. https://doi.org/10.1128/mSystems.00046-17.

34. Cullen, T.W., Schofield, W.B., Barry, N.A., Putnam, E.E., Rundell, E.A., Trent, M.S., Degnan, P.H., Booth, C.J., Yu, H., and Goodman, A.L. (2015). Gut microbiota. Antimicrobial peptide resistance mediates resilience of prominent gut commensals during inflammation. Science *347*, 170–175. https://doi.org/10.1126/science.1260580.

35. Cingöz, O., and Goff, S.P. (2018). Cyclin-dependent kinase activity is required for type I interferon production. Proc. Natl. Acad. Sci. USA *115*, E2950–E2959. https://doi.org/10.1073/pnas.1720431115.

36. Schaupp, L., Muth, S., Rogell, L., Kofoed-Branzk, M., Melchior, F., Lienenklaus, S., Ganal-Vonarburg, S.C., Klein, M., Guendel, F., Hain, T., et al. (2020). Microbiota-Induced Type I Interferons Instruct a Poised Basal State of Dendritic Cells. Cell *181*, 1080–1096.e19. https://doi.org/10.1016/j.cell.2020.04.022.

37. Tan, Y., Zanoni, I., Cullen, T.W., Goodman, A.L., and Kagan, J.C. (2015). Mechanisms of Toll-like Receptor 4 Endocytosis Reveal a Common Immune-Evasion Strategy Used by Pathogenic and Commensal Bacteria. Immunity *43*, 909–922. https://doi.org/10.1016/j.immuni.2015.10.008.

38. Gauthier, A.E., Chandler, C.E., Poli, V., Gardner, F.M., Tekiau, A., Smith, R., Bonham, K.S., Cordes, E.E., Shank, T.M., Zanoni, I., et al. (2021). Deep-sea microbes as tools to refine the rules of innate immune pattern recognition. Sci. Immunol. *6*, eabe0531. https://doi.org/10.1126/sciimmunol.abe0531.

39. Zanoni, I., Ostuni, R., Marek, L.R., Barresi, S., Barbalat, R., Barton, G.M., Granucci, F., and Kagan, J.C. (2011). CD14 controls the LPS-induced endocytosis of Toll-like receptor 4. Cell *147*, 868–880. https://doi.org/10.1016/j.cell.2011.09.051.

40. Huang, Y.L., Morales-Rosado, J., Ray, J., Myers, T.G., Kho, T., Lu, M., and Munford, R.S. (2014). Toll-like receptor agonists promote prolonged triglyceride storage in macrophages. J. Biol. Chem. *289*, 3001–3012. https://doi.org/10.1074/jbc.M113.524587.

41. Bosch, M., Sánchez-Álvarez, M., Fajardo, A., Kapetanovic, R., Steiner, B., Dutra, F., Moreira, L., López, J.A., Campo, R., Marí, M., et al. (2020).

Mammalian lipid droplets are innate immune hubs integrating cell metabolism and host defense. Science *370*, eaay8085. https://doi.org/10.1126/science.aay8085.

42. Tanigawa, K., Suzuki, K., Nakamura, K., Akama, T., Kawashima, A., Wu, H., Hayashi, M., Takahashi, S.I., Ikuyama, S., Ito, T., et al. (2008). Expression of adipose differentiation-related protein (ADRP) and perilipin in macrophages infected with Mycobacterium leprae. FEMS Microbiol. Lett. *289*, 72–79. https://doi.org/10.1111/j.1574-6968.2008.01369.x.

43. Monson, E.A., Crosse, K.M., Duan, M., Chen, W., O'Shea, R.D., Wakim, L. M., Carr, J.M., Whelan, D.R., and Helbig, K.J. (2021). Intracellular lipid droplet accumulation occurs early following viral infection and is required for an efficient interferon response. Nat. Commun. *12*, 4303. https://doi.org/10.1038/s41467-021-24632-5.

44. Monson, E.A., Crosse, K.M., Das, M., and Helbig, K.J. (2018). Lipid droplet density alters the early innate immune response to viral infection. PLoS One *13*, e0190597. https://doi.org/10.1371/journal.pone.0190597.

45. Rajaiah, R., Perkins, D.J., Ireland, D.D.C., and Vogel, S.N. (2015). CD14 dependence of TLR4 endocytosis and TRIF signaling displays ligand specificity and is dissociable in endotoxin tolerance. Proc. Natl. Acad. Sci. USA *112*, 8391–8396. https://doi.org/10.1073/pnas.1424980112.

46. Lakshminarayan, R., Wunder, C., Becken, U., Howes, M.T., Benzing, C., Arumugam, S., Sales, S., Ariotti, N., Chambon, V., Lamaze, C., et al. (2014). Galectin-3 drives glycosphingolipid-dependent biogenesis of clathrin-independent carriers. Nat. Cell Biol. *16*, 595–606. https://doi.org/10.1038/ncb2970.

47. Sabharanjak, S., Sharma, P., Parton, R.G., and Mayor, S. (2002). GPI-anchored proteins are delivered to recycling endosomes via a distinct cdc42-regulated, clathrin-independent pinocytic pathway. Dev. Cell *2*, 411–423. https://doi.org/10.1016/s1534-5807(02)00145-4.

48. Garrett, W.S., Chen, L.M., Kroschewski, R., Ebersold, M., Turley, S., Trombetta, S., Galán, J.E., and Mellman, I. (2000). Developmental control of endocytosis in dendritic cells by Cdc42. Cell *102*, 325–334. https://doi.org/10.1016/s0092-8674(00)00038-6.

49. Mayor, S., and Pagano, R.E. (2007). Pathways of clathrin-independent endocytosis. Nat. Rev. Mol. Cell Biol. *8*, 603–612. https://doi.org/10.1038/nrm2216.

50. Li, Y., Komai-Koma, M., Gilchrist, D.S., Hsu, D.K., Liu, F.T., Springall, T., and Xu, D. (2008). Galectin-3 is a negative regulator of lipopolysaccharide-mediated inflammation. J. Immunol. *181*, 2781–2789. https://doi.org/10.4049/jimmunol.181.4.2781.

51. Nalbant, P., Hodgson, L., Kraynov, V., Toutchkine, A., and Hahn, K.M. (2004). Activation of endogenous Cdc42 visualized in living cells. Science *305*, 1615–1619. https://doi.org/10.1126/science.1100367.

52. Robertson, H., Li, J., Kim, H.J., Rhodes, J.W., Harman, A.N., Patrick, E., and Rogers, N.M. (2021). Transcriptomic Analysis Identifies A Tolerogenic Dendritic Cell Signature. Front. Immunol. *12*, 733231. https://doi.org/10.3389/fimmu.2021.733231.

53. Vander Lugt, B., Riddell, J., Khan, A.A., Hackney, J.A., Lesch, J., DeVoss, J., Weirauch, M.T., Singh, H., and Mellman, I. (2017). Transcriptional determinants of tolerogenic and immunogenic states during dendritic cell maturation. J. Cell Biol. *216*, 779–792. https://doi.org/10.1083/jcb.201512012.

54. Vendelova, E., Ashour, D., Blank, P., Erhard, F., Saliba, A.E., Kalinke, U., and Lutz, M.B. (2018). Tolerogenic Transcriptional Signatures of Steady-State and Pathogen-Induced Dendritic Cells. Front. Immunol. *9*, 333. https://doi.org/10.3389/fimmu.2018.00333.

55. Thornton, A.M., Korty, P.E., Tran, D.Q., Wohlfert, E.A., Murray, P.E., Belkaid, Y., and Shevach, E.M. (2010). Expression of Helios, an Ikaros transcription factor family member, differentiates thymic-derived from peripherally induced Foxp3+ T regulatory cells. J. Immunol. *184*, 3433–3441. https://doi.org/10.4049/jimmunol.0904028.

56. Bhaumik, S., Mickael, M.E., Moran, M., Spell, M., and Basu, R. (2021). RORgammat Promotes Foxp3 Expression by Antagonizing the Effector Program in Colonic Regulatory T Cells. J. Immunol. *207*, 2027–2038. https://doi.org/10.4049/jimmunol.2100175.

57. Yang, B.H., Hagemann, S., Mamareli, P., Lauer, U., Hoffmann, U., Beckstette, M., Föhse, L., Prinz, I., Pezoldt, J., Suerbaum, S., et al. (2016). Foxp3 (+) T cells expressing RORgammat represent a stable regulatory T-cell effector lineage with enhanced suppressive capacity during intestinal inflammation. Mucosal Immunol. *9*, 444–457. https://doi.org/10.1038/mi.2015.74.

58. Gangaplara, A., Martens, C., Dahlstrom, E., Metidji, A., Gokhale, A.S., Glass, D.D., Lopez-Ocasio, M., Baur, R., Kanakabandi, K., Porcella, S. F., et al. (2018). Type I interferon signaling attenuates regulatory T cell function in viral infection and in the tumor microenvironment. PLoS Pathog. *14*, e1006985. https://doi.org/10.1371/journal.ppat.1006985.

59. Metidji, A., Rieder, S.A., Glass, D.D., Cremer, I., Punkosdy, G.A., and Shevach, E.M. (2015). IFN-alpha/beta receptor signaling promotes regulatory T cell development and function under stress conditions. J. Immunol. *194*, 4265–4276. https://doi.org/10.4049/jimmunol.1500036.

60. Tanwar, S., Oguz, C., Metidji, A., Dahlstrom, E., Barbian, K., Kanakabandi, K., Sykora, L., and Shevach, E.M. (2020). Type I IFN signaling in T regulatory cells modulates chemokine production and myeloid derived suppressor cells trafficking during EAE. J. Autoimmun. *115*, 102525. https://doi.org/10.1016/j.jaut.2020.102525.

61. Kedmi, R., Najar, T.A., Mesa, K.R., Grayson, A., Kroehling, L., Hao, Y., Hao, S., Pokrovskii, M., Xu, M., Talbot, J., et al. (2022). A RORgammat (+) cell instructs gut microbiota-specific T(reg) cell differentiation. Nature *610*, 737–743. https://doi.org/10.1038/s41586-022-05089-y.

62. Akagbosu, B., Tayyebi, Z., Shibu, G., Paucar Iza, Y.A., Deep, D., Parisotto, Y.F., Fisher, L., Pasolli, H.A., Thevin, V., Elmentaite, R., et al. (2022). Novel antigen-presenting cell imparts T(reg)-dependent tolerance to gut microbiota. Nature *610*, 752–760. https://doi.org/10.1038/s41586-022-05309-5.

63. Lyu, M., Suzuki, H., Kang, L., Gaspal, F., Zhou, W., Goc, J., Zhou, L., Zhou, J., Zhang, W., et al.; JRI Live Cell Bank (2022). ILC3s select microbiota-specific regulatory T cells to establish tolerance in the gut. Nature *610*, 744–751. https://doi.org/10.1038/s41586-022-05141-x.

64. Berezow, A.B., Ernst, R.K., Coats, S.R., Braham, P.H., Karimi-Naser, L.M., and Darveau, R.P. (2009). The structurally similar, penta-acylated lipopolysaccharides of Porphyromonas gingivalis and Bacteroides elicit strikingly different innate immune responses. Microb. Pathog. *47*, 68–77. https://doi.org/10.1016/j.micpath.2009.04.015.

65. Coyne, M.J., Chatzidaki-Livanis, M., Paoletti, L.C., and Comstock, L.E. (2008). Role of glycan synthesis in colonization of the mammalian gut by the bacterial symbiont Bacteroides fragilis. Proc. Natl. Acad. Sci. USA *105*, 13099–13104. https://doi.org/10.1073/pnas.0804220105.

66. Jain, S., Chang, A.M., Singh, M., McLean, J.S., Coats, S.R., Kramer, R.W., and Darveau, R.P. (2019). Identification of PGN_1123 as the Gene Encoding Lipid A Deacylase, an Enzyme Required for Toll-Like Receptor 4 Evasion, in Porphyromonas gingivalis. J. Bacteriol. *201*. e00683–618. https://doi.org/10.1128/JB.00683-18.

67. Keener, J.E., Goh, B., Yoo, J.S., Oh, S.F., and Brodbelt, J.S. (2024). Top-Down Characterization of Bacterial Lipopolysaccharides and Lipooligosaccharides Using Activated-Electron Photodetachment Mass Spectrometry. Anal. Chem. *96*, 9151–9158. https://doi.org/10.1021/acs.analchem.4c00952.

68. Stewart, C.A., Metheny, H., Iida, N., Smith, L., Hanson, M., Steinhagen, F., Leighty, R.M., Roers, A., Karp, C.L., Müller, W., et al. (2013). Interferon-dependent IL-10 production by Tregs limits tumor Th17 inflammation. J. Clin. Invest. *123*, 4859–4874. https://doi.org/10.1172/JCI65180.

69. Lee, S.E., Li, X., Kim, J.C.K., Lee, J., González-Navajas, J.M., Hong, S.H., Park, I.K., Rhee, J.H., and Raz, E. (2012). Type I interferons maintain Foxp3 expression and T-regulatory cell functions under inflammatory conditions in mice. Gastroenterology *143*, 145–154. https://doi.org/10.1053/j.gastro.2012.03.042.

70. Liu, Y., Yang, M., Tang, L., Wang, F., Huang, S., Liu, S., Lei, Y., Wang, S., Xie, Z., Wang, W., et al. (2022). TLR4 regulates RORgammat(+) regulatory

T-cell responses and susceptibility to colon inflammation through interaction with Akkermansia muciniphila. Microbiome *10*, 98. https://doi.org/10.1186/s40168-022-01296-x.

71. Guo, B., Chang, E.Y., and Cheng, G. (2008). The type I IFN induction pathway constrains Th17-mediated autoimmune inflammation in mice. J. Clin. Invest. *118*, 1680–1690. https://doi.org/10.1172/JCI33342.
72. Shinohara, M.L., Kim, J.H., Garcia, V.A., and Cantor, H. (2008). Engagement of the type I interferon receptor on dendritic cells inhibits T helper 17 cell development: role of intracellular osteopontin. Immunity *29*, 68–78. https://doi.org/10.1016/j.immuni.2008.05.008.
73. Kavrochorianou, N., Evangelidou, M., Markogiannaki, M., Tovey, M., Thyphronitis, G., and Haralambous, S. (2016). IFNAR signaling directly modulates T lymphocyte activity, resulting in milder experimental autoimmune encephalomyelitis development. J. Leukoc. Biol. *99*, 175–188. https://doi.org/10.1189/jlb.3A1214-598R.
74. Gessani, S., Conti, L., Del Cornò, M., and Belardelli, F. (2014). Type I interferons as regulators of human antigen presenting cell functions. Toxins (Basel) *6*, 1696–1723. https://doi.org/10.3390/toxins6061696.
75. Fujimoto, Y., Ochi, H., Maekawa, T., Abe, H., Hayes, C.N., Kumada, H., Nakamura, Y., and Chayama, K. (2011). A single nucleotide polymorphism in activated Cdc42 associated tyrosine kinase 1 influences the interferon therapy in hepatitis C patients. J. Hepatol. *54*, 629–639. https://doi.org/10.1016/j.jhep.2010.07.021.
76. Mazouz, N., Detournay, O., Buelens, C., Renneson, J., Trakatelli, M., Lambermont, M., Goldman, M., and Tougouz, M. (2005). Immunostimulatory properties of human dendritic cells generated using IFN-beta associated either with IL-3 or GM-CSF. Cancer Immunol. Immunother. *54*, 1010–1017. https://doi.org/10.1007/s00262-005-0664-7.
77. Saitoh, T., Satoh, T., Yamamoto, N., Uematsu, S., Takeuchi, O., Kawai, T., and Akira, S. (2011). Antiviral protein Viperin promotes Toll-like receptor 7- and Toll-like receptor 9-mediated type I interferon production in plasmacytoid dendritic cells. Immunity *34*, 352–363. https://doi.org/10.1016/j.immuni.2011.03.010.
78. Olszak, T., Neves, J.F., Dowds, C.M., Baker, K., Glickman, J., Davidson, N.O., Lin, C.S., Jobin, C., Brand, S., Sotlar, K., et al. (2014). Protective mucosal immunity mediated by epithelial CD1d and IL-10. Nature *509*, 497–502. https://doi.org/10.1038/nature13150.
79. Proenca-Modena, J.L., Sesti-Costa, R., Pinto, A.K., Richner, J.M., Lazear, H.M., Lucas, T., Hyde, J.L., and Diamond, M.S. (2015). Oropouche virus infection and pathogenesis are restricted by MAVS, IRF-3, IRF-7, and type I interferon signaling pathways in nonmyeloid cells. J. Virol. *89*, 4720–4737. https://doi.org/10.1128/JVI.00077-15.
80. Hubbard, N.W., Ames, J.M., Maurano, M., Chu, L.H., Somfleth, K.Y., Gokhale, N.S., Werner, M., Snyder, J.M., Lichauco, K., Savan, R., et al. (2022). ADAR1 mutation causes ZBP1-dependent immunopathology. Nature *607*, 769–775. https://doi.org/10.1038/s41586-022-04896-7.
81. Mutemberezi, V., Buisseret, B., Masquelier, J., Guillemot-Legris, O., Alhouayek, M., and Muccioli, G.G. (2018). Oxysterol levels and metabolism in the course of neuroinflammation: insights from in vitro and in vivo models. J. Neuroinflammation *15*, 74. https://doi.org/10.1186/s12974-018-1114-8.
82. García-Bayona, L., and Comstock, L.E. (2019). Streamlined Genetic Manipulation of Diverse Bacteroides and Parabacteroides Isolates from the Human Gut Microbiota. mBio *10*, e01762-19. https://doi.org/10.1128/mBio.01762-19.
83. Lim, B., Zimmermann, M., Barry, N.A., and Goodman, A.L. (2017). Engineered Regulatory Systems Modulate Gene Expression of Human Commensals in the Gut. Cell *169*, 547–558.e15. https://doi.org/10.1016/j.cell.2017.03.045.
84. Cho, H.S., Shin, H.M., Haberstock-Debic, H., Xing, Y., Owens, T.D., Funk, J.O., Hill, R.J., Bradshaw, J.M., and Berg, L.J. (2015). A Small Molecule Inhibitor of ITK and RLK Impairs Th1 Differentiation and Prevents Colitis Disease Progression. J. Immunol. *195*, 4822–4831. https://doi.org/10.4049/jimmunol.1501828.
85. Zhang, H., Madi, A., Yosef, N., Chihara, N., Awasthi, A., Pot, C., Lambden, C., Srivastava, A., Burkett, P.R., Nyman, J., et al. (2020). An IL-27-Driven Transcriptional Network Identifies Regulators of IL-10 Expression across T Helper Cell Subsets. Cell Rep. *33*, 108433. https://doi.org/10.1016/j.celrep.2020.108433.
86. Matyash, V., Liebisch, G., Kurzchalia, T.V., Shevchenko, A., and Schwudke, D. (2008). Lipid extraction by methyl-tert-butyl ether for high-throughput lipidomics. J. Lipid Res. *49*, 1137–1146. https://doi.org/10.1194/jlr.D700041-JLR200.
87. Shimoyama, A., Di Lorenzo, F., Yamaura, H., Mizote, K., Palmigiano, A., Pither, M.D., Speciale, I., Uto, T., Masui, S., Sturiale, L., et al. (2021). Lipopolysaccharide from Gut-Associated Lymphoid-Tissue-Resident Alcaligenes faecalis: Complete Structure Determination and Chemical Synthesis of Its Lipid A. Angew. Chem. Int. Ed. Engl. *60*, 10023–10031. https://doi.org/10.1002/anie.202012374.
88. Xue, J., Han, Z., Li, G., Emmanuel, K.A., McManus, C.L., Sui, Q., Ge, D., Gao, Q., and Cai, L. (2020). Synthesis of monophosphorylated lipid A precursors using 2-naphthylmethyl ether as a protecting group. Beilstein J. Org. Chem. *16*, 1955–1962. https://doi.org/10.3762/bjoc.16.162.
89. Fujimoto, Y., Shimoyama, A., Saeki, A., Kitayama, N., Kasamatsu, C., Tsutsui, H., and Fukase, K. (2013). Innate immunomodulation by lipophilic termini of lipopolysaccharide; synthesis of lipid As from Porphyromonas gingivalis and other bacteria and their immunomodulative responses. Mol. Biosyst. *9*, 987–996. https://doi.org/10.1039/c3mb25477a.

Please cite this article in press as: Cho et al., Structure of gut microbial glycolipid modulates host inflammatory response, Cell (2025), https://doi.org/10.1016/j.cell.2025.05.016

STAR★METHODS

KEY RESOURCES TABLE

REAGENT or RESOURCE	SOURCE	IDENTIFIER
Antibodies		
Alexa Fluor 488 anti-mouse GATA-3	BioLegend	Cat # 653808; RRID: AB_2563215;
Alexa Fluor 647 anti-mouse AIRE	BioLegend	Cat# 567253; RRID: AB_2916515
Alexa Fluor 700 anti-mouse CD4	BD Biosciences	Cat # 557956; RRID: AB_396956
Alexa Fluor 700 anti-mouse CD11c	BioLegend	Cat# 117320; RRID: AB_528736
Alexa Fluor 700 anti-mouse CD90.2	BioLegend	Cat# 105320; RRID: AB_493725
Alexa Fluor 700 anti-mouse TCRβ	BioLegend	Cat# 109224; RRID: AB_1027648
PerCP/Cy5.5 anti-mouse CD3ε	BioLegend	Cat# 100217; RRID: AB_1595597
APC anti-mouse CD103	BioLegend	Cat# 121414; RRID: AB_1227502
APC anti-mouse CD170	BioLegend	Cat# 155508; RRID: AB_2750237
APC anti-mouse CD274	BioLegend	Cat# 124312; RRID: AB_10612741
APC anti-mouse CD284/MD2	BioLegend	Cat# 145406; RRID: AB_2562503
APC anti-mouse Foxp3	Invitrogen	Cat# 17-5773-82; RRID: AB_469457
APC anti-mouse/human IL-5	BioLegend	Cat# 504306; RRID: AB_315330
APC anti-mouse RORγt	Invitrogen	Cat# 17-6981-82; RRID: AB_2573254
APC/Cy7 anti-mouse CD3ε	BioLegend	Cat# 100330; RRID: AB_1877170
APC/Cy7 anti-mouse CD4	BioLegend	Cat# 100413; RRID: AB_312698
APC/Cy7 anti-mouse CD62L	BioLegend	Cat# 104428; RRID: AB_830799
APC/Cy7 anti-mouse CD86	BioLegend	Cat# 105030; RRID: AB_2244452
APC/Cy7 anti-mouse TCRβ	BioLegend	Cat# 109220; RRID: AB_893624
APC/Cy7 anti-mouse NK1.1	BioLegend	Cat# 108724; RRID: AB_830871
APC/Cy7 Streptavidin	BioLegend	Cat# 405208
Biotin anti-mouse CD275	BioLegend	Cat# 107403; RRID: AB_345259
BUV563 anti-mouse Ly-6G	BD Biosciences	Cat# 612974; Clone 1A8
BUV615 anti-mouse CD11b	Invitrogen	Cat# 366-0112-82; RRID: AB_3074009
BUV661 anti-mouse CD4	BD Biosciences	Cat# 612974; RRID: AB_2870246
BUV661 anti-mouse CD317	BD Biosciences	Cat# 750635; RRID: AB_2874766
BUV737 anti-mouse CD45	BD Biosciences	Cat# 748371; RRID: AB_2872790
BUV805 anti-mouse CD103	BD Biosciences	Cat# 741948; RRID: AB_2871259
BV421 anti-mouse Siglec-F	BD Biosciences	Cat# 562681; RRID: AB_2722581
BV510 anti-mouse TCRγδ	BioLegend	Cat# 118131; RRID: AB_2563534
BV605 anti-mouse CD4	BioLegend	Cat# 100548; RRID: AB_2563054
BV605 anti-mouse CD11c	BioLegend	Cat# 117334; RRID: AB_2562415
BV711 anti-mouse CD4	BD Biosciences	Cat# 563726; RRID: AB_2738389
BV711 anti-mouse CD64	BD Biosciences	Cat# 139311; RRID: AB_2563846
BV750 anti-mouse CD4	BD Biosciences	Cat# 747203; RRID: AB_2871929
BV750 anti-mouse TCRγδ	BD Biosciences	Cat# 746962; RRID: AB_2871745
eFluor 450 anti-mouse CD19	Invitrogen	Cat# 48-0193-82; RRID: AB_2734905
eFluor 450 anti-mouse CD127	Invitrogen	Cat# 48-1271-82; RRID: AB_2016698
eFluor 450 anti-mouse IL-13	Invitrogen	Cat# 48-7133-82; RRID: AB_11219690
FITC anti-mouse CD3ε	BioLegend	Cat# 100306; RRID: AB_312671
FITC anti-mouse CD11c	BioLegend	Cat# 117306; RRID: AB_313775
FITC anti-mouse CD40	BioLegend	Cat# 124608; RRID: AB_1134096

(*Continued on next page*)

Please cite this article in press as: Cho et al., Structure of gut microbial glycolipid modulates host inflammatory response, Cell (2025), https://doi.org/10.1016/j.cell.2025.05.016

Continued

REAGENT or RESOURCE	SOURCE	IDENTIFIER
FITC anti-mouse CD90.2	BioLegend	Cat# 140304; RRID: AB_10642812
FITC anti-mouse CD103	BioLegend	Cat# 121420; RRID: AB_10714791
FITC anti-mouse CD170	BioLegend	Cat# 155504; RRID: AB_2750233
FITC anti-mouse IL-17A	BioLegend	Cat# 506908; RRID: AB_536010
Pacific Blue anti-mouse CD3ε	BioLegend	Cat# 100214; RRID: AB_493645
Pacific Blue anti-mouse CD11c	BioLegend	Cat# 117322; RRID: AB_755988
Pacific Blue anti-mouse CD80	BioLegend	Cat# 104724; RRID: AB_2075999
Pacific Blue anti-mouse Helios	BioLegend	Cat# 137220; RRID: AB_10690535
PE anti-mouse CD11b	BioLegend	Cat# 101208; RRID: AB_312791
PE anti-mouse CD45R/B220	BioLegend	Cat# 103207; RRID: AB_312992
PE anti-mouse CD273	BioLegend	Cat# 107206; RRID: AB_2162011
PE anti-mouse CD282	BioLegend	Cat# 148604; RRID: AB_2564120
PE anti-mouse GATA-3	BioLegend	Cat# 653804; RRID: AB_2562723
PE anti-mouse IFNAR1	Invitrogen	Cat# 12-5945-82; RRID: AB_2572646
PE anti-mouse RORγt	Invitrogen	Cat# 12-6981-82; RRID: AB_10807092
PE-CF594 anti-mouse CD14	BD Biosciences	Cat# 564145; RRID: AB_2738619
PE-CF594 anti-mouse CD45R/B220	BD Biosciences	Cat# 562313; RRID: AB_11151901
PE/Cy7 anti-mouse CD86	BioLegend	Cat# 105014; RRID: AB_439783
PE/Cy7 anti-mouse CD284/MD2	BioLegend	Cat# 117610; RRID: AB_2044020
PE/Cy7 anti-mouse F4/80	BioLegend	Cat# 123114; RRID: AB_893478
PE/Cy7 anti-mouse IL-10	BioLegend	Cat# 505026; RRID: AB_11150582
PE/Cy7 anti-mouse T-bet	BioLegend	Cat# 644824; RRID: AB_2561761
PE/Cy7 anti-mouse TCRβ	BioLegend	Cat# 109222; RRID: AB_893625
PE-TexasRed anti-mouse CD19	Invitrogen	Cat# RM7717; RRID: AB_10373569
PE-TexasRed anti-mouse CD8a	Invitrogen	Cat# MCD0817; RRID: AB_2869989
PE-TexasRed anti-mouse CD19	Invitrogen	Cat# MHCD1917; RRID: AB_10372040
PE-TexasRed anti-mouse CD45	Invitrogen	Cat# MCD4517; RRID: AB_10392557
PerCP/Cy5.5 anti-mouse CD3ε	BioLegend	Cat# 100217; RRID: AB_1595597
PerCP/Cy5.5 anti-mouse CD274	BioLegend	Cat# 124334; RRID: AB_2629832
PerCP/Cy5.5 anti-mouse CD317	BioLegend	Cat# 127022; RRID: AB_2566647
PerCP/Cy5.5 anti-mouse IFN-γ	BioLegend	Cat# 505822; RRID: AB_961359
PerCP/Cy5.5 anti-mouse Ly-6C	BioLegend	Cat# 128012; RRID: AB_1659241
PerCP/Cy5.5 anti-mouse T-bet	BioLegend	Cat# 644806; RRID: AB_1595488
PerCP/Cy5.5 anti-mouse TCRγ/δ	BioLegend	Cat# 118118; RRID: AB_10612756
V500 anti-mouse CD3ε	BioLegend	Cat# 560771; RRID: AB_1937314
V500 anti-mouse CD44	BD Biosciences	Cat# 560780; RRID: AB_1937328
V500 anti-mouse I-A/I-E	BD Biosciences	Cat# 562366; RRID: AB_11153488
PE anti-mouse TLR4 (CD284)	BioLegend	Cat# 117610; RRID: AB_2044020
PE/Cy7 anti-mouse TLR4 (CD284)	BioLegend	Cat# 117606; RRID: AB_2205138
anti-Lipid A antibody	Abcam	Cat# ab8467; Clone 26-5
Goat anti-mouse IgM Secondary Antibody, HRP	Invitrogen	Cat# 31440; RRID: AB_228329
anti-mouse Galectin 3 monoclonal antibody	Invitrogen	Cat# 14-5301-82; RRID: AB_837132
Functional Grade, anti-mouse IFN-γ monoclonal antibody	Invitrogen	Cat# 16-7311-81; RRID: AB_469242
Functional Grade, anti-mouse IL-2 monoclonal antibody	Invitrogen	Cat# 16-7022-81; RRID: AB_469206

(*Continued on next page*)

Please cite this article in press as: Cho et al., Structure of gut microbial glycolipid modulates host inflammatory response, Cell (2025), https://doi.org/10.1016/j.cell.2025.05.016

Continued

REAGENT or RESOURCE	SOURCE	IDENTIFIER
Functional Grade, anti-mouse IL-4 monoclonal antibody	Invitrogen	Cat# 16-7041-81; RRID: AB_469208
Bacterial and Viral Strains		
Escherichia coli K12 strain	This paper	N/A
Bacteroides fragilis NCTC 9343	This paper	N/A
Bacteroides fragilis Acapsular mutant (*ΔungD1 ΔungD2 ΔPSH*)	Laurie Comstock (University of Chicago)[65]	N/A
Bacteroides fragilis Acapsular mutant inducbily expressing BF0187 (Acap_BF0187)	This paper	N/A
Bacteroides caccae ATCC 43185	This paper	N/A
Bacteroides cellulosilyticus DSM 14838	This paper	N/A
Bacteroides dorei DSM 17855	This paper	N/A
Bacteroides finegoldii DSM 17565	This paper	N/A
Bacteroides nordii CL02T12C05	This paper	N/A
Bacteroides ovatus ATCC 8483	This paper	N/A
Bacteroides salanitronis DSM 18170	This paper	N/A
Bacteroides salyersiae CL02T12C01	This paper	N/A
Bacteroides thetaiotaomicron ATCC 29148	This paper	N/A
Bacteroides uniformis ATCC 8492	This paper	N/A
Bacteroides vulgatus ATCC 8482	This paper	N/A
Bacteroides xylanisolvens CL30T12C04	This paper	N/A
Biological Samples		
Ultrapure LPS from *Escherichia coli* K12	InvivoGen	tlrl-peklps
Ultrapure LPS from *Escherichia coli* 0111:B4	InvivoGen	tlrl-3pelps
Ultrapure LPS from *Escherichia coli* 055:B5	InvivoGen	tlrl-pb5lps
Ultrapure LPS from *Salmonella minnesota* R595	InvivoGen	tlrl-smflps
Ultrapure LPS from *Porphyromonas gingivalis*	InvivoGen	tlrl-ppflps
Ultrapure LPS from *Rhodobacter sphaeroides*	InvivoGen	tlrl-prslps
LOS purified from *Bacteroides fragilis* NCTC 9343	This paper	N/A
LOS purified from *Bacteroides fragilis* Acapsular mutant (*ΔungD1 ΔungD2 ΔPSH*)	This paper	N/A
LOS purified from *Bacteroides fragilis* Acapsular mutant inducibly expressing BF0187 (Acap_BF0187)	This paper	N/A
LOS purified from *Bacteroides fragilis ΔarnT*	This paper	N/A
LOS purified from *Bacteroides caccae* ATCC 43185	This paper	N/A
LOS purified from *Bacteroides cellulosilyticus* DSM 14838	This paper	N/A
LOS purified from *Bacteroides dorei* DSM 17855	This paper	N/A
LOS purified from *Bacteroides finegoldii* DSM 17565	This paper	N/A
LOS purified from *Bacteroides nordii* CL02T12C05	This paper	N/A
LOS purified from *Bacteroides ovatus* ATCC 8483	This paper	N/A
LOS purified from *Bacteroides salanitronis* DSM 18170	This paper	N/A
LOS purified from *Bacteroides salyersiae* CL02T12C01	This paper	N/A
LOS purified from *Bacteroides thetaiotaomicron* ATCC 29148	This paper	N/A
LOS purified from *Bacteroides uniformis* ATCC 8492	This paper	N/A
LOS purified from *Bacteroides vulgatus* ATCC 8482	This paper	N/A
LOS purified from *Bacteroides xylanisolvens* CL30T12C04	This paper	N/A

(*Continued on next page*)

Please cite this article in press as: Cho et al., Structure of gut microbial glycolipid modulates host inflammatory response, Cell (2025), https://doi.org/10.1016/j.cell.2025.05.016

Continued

REAGENT or RESOURCE	SOURCE	IDENTIFIER
Chemicals, Peptides, and Recombinant Proteins		
Amiloride hydrochloride	Millipore-Sigma	1019701-500MG
Casin	Millipore-Sigma	SML1253-5MG
Chloropromazine hydrochloride	Millipore-Sigma	C8138-5G
Dynasore hydrate	Millipore-Sigma	D7693-5MG
Genistein	Millipore-Sigma	G6649-5MG
Nystatin	Millipore-Sigma	1477003-200MG
BODIPY 493/503 (4,4-Difluoro-1,3,5,7, 8-Pentamethyl-4-Bora-3a,4a-Diaza-s-Indacene)	Invitrogen	D3922
AZD 3988	Tocris Bioscience	4837
Dextran Sodium Sulfate Salt, Colitis Grade (MW 36,000-50,000)	MP Biomedicals	MFCD00081551
Monophosphoryl Tri-acyl Lipid A (3A-MPLA)	Avanti Polar Lipids	699851
Monophosphoryl Tetra-acyl Lipid A (4A-MPLA)	Avanti Polar Lipids	699854
Monophosphoryl 3-Deacyl Lipid A (5A-MPLA)	Avanti Polar Lipids	699852
Lipid A (*Escherichia coli*) (6A-DPLA)	Vivitide (now Biosynth)	CLP-24005-s
s5A-MP-C80	This paper	N/A
s4A-MP-C68	This paper	N/A
s4A-MP-C64_1	This paper	N/A
s4A-MP-C64_2	This paper	N/A
s3A-MP-C60	This paper	N/A
Collagenase, Type II	Gibco	17101015
Collagnease D from *Clostrium histolyticum*	Roche	11088866001
Dispase II	Gibco	17105041
Dithiothreitol	Millipore-Sigma	D0632-10G
Percoll	Cytivia	GE17-0891-01
UltraPure 0.5M EDTA, pH 8.0	Gibco	15575020
Live/Dead Fixable Yellow Dead Cell Stain Kit	Invitrogen	L34967
Fluoresbrite YG Carboxylate Microsphere (1.0μm)	Polysciences	15702-10
Vancomycin Hydrochloride	ThermoFisher Scientific	J62790
Neomycin Trisulfate Salt Hydrate	Millipore Sigma	N6386
Metronidazole Benzoate	AstaTech	C90395
Ampicillin Trihydrate	Millipore Sigma	A1593
UltraPure Tris-HCl (pH 8.0)	Invitrogen	15568025
10% UltraPure SDS Solution	Thermo Scientific	24730020
2-Mercaptoethanol	Thermo Scientific	125472500
$MgCl_2$	Sigma-Aldrich	M8266
Proteinase K	Millipore	70663
3 M Sodium Acetate Solution, Molecular Biology Grade	Millipore	567422
Ethanol	Sigma-Aldrich	459844
DNase I	Invitrogen	18047019
RNase A	Invitrogen	EN0531
UltraPure Buffer-Saturated Phenol	Invitrogen	15513047
HyClone Water, Cell Culture Grade (Endotoxin-Free)	Cytivia	SH30529
2-Propanol	Sigma-Aldrich	1027814000
Acetonitrile	Sigma-Aldrich	AX0156
Formic Acid	Sigma-Aldrich	100264500

(*Continued on next page*)

Please cite this article in press as: Cho et al., Structure of gut microbial glycolipid modulates host inflammatory response, Cell (2025), https://doi.org/10.1016/j.cell.2025.05.016

Continued

REAGENT or RESOURCE	SOURCE	IDENTIFIER
NEBuilder HiFi DNA Assembly Cloning Kit	New England BioLabs	E5520S
Brucella Agar with 5% Sheep Blood, Hemin, and Vitamin K	Thermo Scientific	R01254
Brain Heart Infusion Agar	Anaerobe Systems	AS-6426
NaCl	Sigma-Aldrich	S9888
D-(+)-Glucose	Thermo Scientific Chemicals	A16828.0C
K_2HPO_4	Sigma-Aldrich	P3786
L-Cysteine	Thermo Scientific Chemicals	AAA1043518
Ampicillin	Sigma-Aldrich	A9393
Erythromycin	Sigma-Aldrich	E0774
Gentamycin	Gibco	15750060
Anhydrotetracycline Hydrochloride	Sigma-Aldrich	1035708
OVA Peptide (323-339)	GenScript	RP10610
Recombinant Human TLR4/MD2 Complex Protein	R&D Systems	3146-TM-050/CF
Ni-NTA HisSorb Plates	QIAGEN	35061
all-*trans*-Retinoic acid	Millipore-Sigma	R2625-50MG
GolgiPlug Protein Transport Inhibitor (Bredfeldin A)	BD Biosciences	555029
GolgiStop Protein Transport Inhibitor (Monensin)	BD Biosciences	554724
Ionomycin from *Streptomyces conglobatus*	Millipore-Sigma	I9657-1MG
Phorbol 12-myristate 13-acetate	Millipore-Sigma	79346-1MG
Recombinant mouse IL-1β, Carrier-free	R&D Systems	401-ML-005/CF
Recombinant mouse IL-2, Carrier-free	R&D Systems	402-ML-020/CF
Recombinant mouse IL-4, Carrier-free	R&D Systems	404-ML-010/CF
Recombinant mouse IL-6, Carrier-free	R&D Systems	406-ML-005/CF
Recombinant mouse IL-12, Carrier-free	R&D Systems	419-ML-010/CF
Recombinant mouse IL-23, Carrier-free	R&D Systems	1887-ML-010/CF
Recombinant mouse IL-27, Carrier-free	R&D Systems	2799-ML/CF
Recombinant mouse TGF-β1, Carrier-free	R&D Systems	7666-MB-005/CF
Recombinant mouse GM-CSF	Peprotech	315-03
ACK Lysis Buffer	Gibco	A1049201
Trypan Blue Solution, 0.4%	Gibco	15250061
Foxp3 Transcription Factor Fixation/Permeabilization Concentrate and Diluent	Invitrogen	00-5521-00
Fixation Buffer	BD Biosciences	554655
IC Fixation Buffer	Invitrogen	00-8222-49
BD GolgiPlug Protein Transport Inhbhtor (Brefeldin A)	BD Biosciences	555029
BD GolgiStop Protein Transport Inhbhtor (Monensin)	BD Biosciences	554724
LIVE/DEAD Fixable Yellow Dead Cell Stain Kit	Invitrogen	L34959
TLC Silica gel 60 F_{254}	EMD Millipore	105554
Siica gel high-purity grade 9385, pore size 60 Å, 230-400 mesh particle size	EMD Millipore	60737
p-Anisaldehyde	Millipore-Sigma	A88107
Potassium permanganate	ThermoFisher Scientific	035590.K7
Phosphomolybdic acid	Millipore-Sigma	221856
Permeabilization Buffer (10X)	Invitrogen	00-8333-56
NEBuilder HiFi DNA Assembly Cloning Kit	New England BioLabs	E5520S
GlycoBlue Coprecipitant	Invitrogen	AM9516
iTaq Universal SYBR Green Supermix	Bio-Rad	1725124

(*Continued on next page*)

Please cite this article in press as: Cho et al., Structure of gut microbial glycolipid modulates host inflammatory response, Cell (2025), https://doi.org/10.1016/j.cell.2025.05.016

Continued

REAGENT or RESOURCE	SOURCE	IDENTIFIER
TRIzol Reagent	Invitrogen	15596018
PrimeScript RT Reagent Kit	Takara	RR037A
NEBNext Poly(A) mRNA Magnetic Isolation Module	New England BioLabs	E7490L
NEBNExt Ultra II Directional RNA Libaray Prep with Sample Purification Beads	New England BioLabs	E7765S
NEBNExt Multiplex Oligos for Illumina (Index Primers Set 1)	New England BioLabs	E7335S
NEBNExt Multiplex Oligos for Illumina (Index Primers Set 2)	New England BioLabs	E7500S
NEBNExt Multiplex Oligos for Illumina (Index Primers Set 3)	New England BioLabs	E7710S
Critical Commercial Assays		
CellTrace Violet Cell Proliferation Kit for Flow Cytometry	Invitrogen	C34557
CD4+ T cell Isolation Kit, Mouse	Miltenyi Biotec	130-095-248
CD11c MicroBeads UltraPure, Mouse	Miltenyi Biotec	130-125-835
Mouse IL-6 Quantikine ELISA Kit	R&D Systems	M6000B
Mouse IL-10 Quantikine ELISA Kit	R&D Systems	M1000B
Mouse IFN-beta Quantikine ELISA Kit	R&D Systems	MIFNB0
Mouse TNF-alpha Quantikine ELISA Kit	R&D Systems	MTA00B
Intracellular pH Calibration Buffer Kit	Invitrogen	P35379
pHrodo Green AM Intracellular pH Indicator Dyes	Invitrogen	P35373
Deposited Data		
Bulk RNA-Seq data	This Paper	GEO: GSE296696
Experimental Models: Organisms/Strains		
C57BL/6J WT	JAX	000664
B6(Cg)-*Tlr4tm1.2Karp*/J	JAX	029015
B6.129P-*Tlr2tm1Kir*/J	JAX	004650
B6.129P2(SJL)-*Myd88tm1.1Defr*/J	JAX	009088
C57BL/6J-*Ticam1Lps2*/J	JAX	005037
B6.129S2-*Ifnar1tm1Agt*/Mmjax	MMRRC (KOMP)	032045-JAX
B6(Cg)-*Ifnar1tm1.1Ees*/J	JAX	028256
B6.129-*Ifnb1tm1Lky*/J	JAX	010818
B6.129(Cg)-*Foxp3tm4(YFP/icre)Ayr*/J	JAX	016959
B6(Cg)-*Rorctm3Litt*/J	JAX	008771
B6.Cg-*Rag2tm1.1Cgn*/J	JAX	008449
C57BL/6NTac.Cg-*Rag2tm1Fwa Il2rgtm1Wji*	Taconic	4111-M/F
B6.129P2-*Tcrbtm1Mom*/J	JAX	002118
B6 Foxp3^{hCd2} x Il10^{Venus} Dual Reporter Mice	Sarkis Mazmanian (CalTech)	N/A
Oligonucleotides		
mActb Forward 5'-GATGCTCCCCGGGCTGTATT-3'	Olszak et al.[78]	N/A
mActb Reverse 5'-GGGGTACTTCAGGGTCAGGA-3'	Olszak et al.[78]	N/A
mIfna Forward 5'-CTTCCACAGGATCACTGTGTACCT-3'	Proenca-Modena et al.[79]	N/A
mIfna Reverse 5'-TTCTGCTCTGACCACCTCCC-3'	Proenca-Modena et al.[79]	N/A
mIfnb Forward 5'-CTGGAGCAGCTGAATGGAAAG-3'	Hubbard et al.[80]	N/A
mIfnb Reverse 5'-CTTCTCCGTCATCTCCATAGGG-3'	Hubbard et al., 2015[80]	N/A
mIl6 Forward 5'-ACAAGTCGGAGGCTTAATTACACAT-3'	Mutemberezi et al.[81]	N/A
mIl6 Reverse 5'-AATCAGAATTGCCATTGCACAA-3'	Mutemberezi et al.[81]	N/A

(*Continued on next page*)

Please cite this article in press as: Cho et al., Structure of gut microbial glycolipid modulates host inflammatory response, Cell (2025), https://doi.org/10.1016/j.cell.2025.05.016

Continued

REAGENT or RESOURCE	SOURCE	IDENTIFIER
Recombinant DNA		
pLGB13	Addgene; García-Bayona and Comstock[82]	Plasmid #126618
pNBU2 erm-TetR-P1T_DP-GH023	Addgene; Lim et al.[83]	Plasmid #90324
Software and Algorithms		
FlowJo v10.9	BD Biosciences	N/A
GraphPad Prism v10.0.3 (217)	GraphPad Software	N/A
Harvard Meidcal School O2 High Performance Compute Cluster	https://it.hms.harvard.edu/our-services/research-computing	N/A
Qualimap	http://qualimap.conesalab.org/	N/A
FastQC	https://www.bioinformatics.babraham.ac.uk/projects/fastqc/	N/A
SAMtools	https://samtools.sourceforge.net/	N/A
STAR Aligner	https://github.com/alexdobin/STAR	N/A
MORPHEUS	https://software.broadinstitute.org/morpheus	N/A
STRING	https://string-db.org/	N/A
DESeq2	https://bioconductor.org/packages/release/bioc/html/DESeq2.html	N/A
R v4.2.1	https://r-project.org	N/A
ggplot2	https://ggplot2.tidyverse.org/	N/A
Enrichr	https://maayanlab.cloud/Enrichr/	N/A
Other		
BD LSR II	BD Biosciences	339101
BD FACSymphony A5 SE Cell Analyzer	BD Biosciences	BD FACSymphony A5 SE
ChemiDoc MP Imaging System	Bio-Rad	12003154
Biotek Synergy HT Microplate Reader	Biotek	309647
NanoDrop 2000	Thermo Scientific	ND-2000
Thermo Vanquish UHPLC	Thermo Scientific	IQLAAAGABHFAPUMZZZ
Q Exactive Orbitrap Mass Spectrometer	Thermo Scientific	0726090
GlassContour Ultimate Solvent Purification System	Nikko Hansen & Co., Ltd.	N/A
NE-300 Just Infusion Syringe Pump	New Era Pump Systems	NE-300
Isolera One Flash Chromatograph	Biotage	ISO-1SV
Siica gel high-purity grade 9385, pore size 60 Å, 230–400 mesh particle size	EMD Millipore	60737
LCMS-2020 Single Quadrupole LC/MS	Shimadzu	LCMS-2020
Bruker Avance III HD 500 MHz NMR Spectroscopy	Bruker	Avance III HD 500
UltrafleXtreme MALDI TOF/TOF Mass Spectrometer	Bruker	UT0274H101
QuantStudio 5 Real-Time PCR	Applied Biosystems	A34322

EXPERIMENTAL MODEL AND SUBJECT DETAILS

Mice

C57BL/6J WT (RRID: IMSR_JAX:000664), B6(Cg)-*Tlr4*$^{tm1.2Karp}$/J (RRID: IMSR_JAX:029015), B6.129P-*Tlr2*^{tm1Kir}/J (RRID: IMSR_JAX:004650), B6.129P2(SJL)-*Myd88*$^{tm1.1Defr}$/J (RRID: IMSR_JAX:009088), C57BL/6J-*Ticam1*^{Lps2}/J (RRID: IMSR_JAX:005037), B6.129S2-*Ifnar1*^{tm1Agt}/Mmjax (RRID: MMRRC_032045-JAX), B6(Cg)-*Ifnar1*$^{tm1.1Ees}$/J (RRID: IMSR_JAX:028256), B6.129-*Ifnb1*^{tm1Lky}/J (RRID: IMSR_JAX:010818), B6.129(Cg)-*Foxp3*$^{tm4(YFP/icre)Ayr}$/J (RRID: IMSR_JAX:016959), B6(Cg)-*Rorctm3Litt*/J (RRID: IMSR_JAX: 008771), B6.Cg-*Rag2*$^{tm1.1Cgn}$/J (RRID: IMSR_JAX:008449), C57BL/6NTac.Cg-*Rag2*^{tm1Fwa} *Il2rg*^{tm1Wji} (Taconic, 4111-M/F), B6.129P2-*Tcrbtm1Mom*/J (RRID: IMSR_JAX: 002118), and B6 *Foxp3*^{hCd2} *Il10*^{Venus} (Sarkis Mazmanian, CalTech) mice were bred and housed under SPF conditions at the Harvard Medical School Animal Facility. Both male and female WT and genetically

Please cite this article in press as: Cho et al., Structure of gut microbial glycolipid modulates host inflammatory response, Cell (2025), https://doi.org/10.1016/j.cell.2025.05.016

modified mice were equally used in age- and sex-matched groups, typically 6 to 10 weeks. All performed experiments were in accordance with the guideline approved by the Harvard Medical Area Standing Committee on Animals.

mBMDC Culture

BM precursors were isolated from the tibia and femur of B6 SPF WT male or female mice (6-10 weeks old) by flushing the cavity of marrow with serum-free RPMI 1640 medium (Gibco). Red blood cells (RBCs) from the harvested BM cells were lysed with ACK Lysing Buffer (Invitrogen), washed with complete medium, and then stained with 0.4% Trypan Blue (Invitrogen) for cell counting. 2.0 x 10^6 cells of BM cells were plated in 10 cm tissue culture plate and cultured for 9 days in the presence of 20 ng/mL murine GM-CSF (PeproTech) while the medium was changed in every 3 days. Loosely attached or semi-suspended cells in the plate were collected and counted.

T cell Proliferation Assay

Excised spleen from naïve B6 SPF WT male or female mice (6-8 weeks old) was chopped off by 4-5 pieces and then digested by 5.0 mL of complete RPMI 1640 dissolved with Collagenase D (1.0 mg/mL) (Sigma-Aldrich) for 30 min at 37°C. Digested pieces were grinded on the 40 μm Cell Strainer using the plunger of syringe. After RBC digestion with ACK Lysis Buffer, the digested tissues were labeled with the mouse CD11c MicroBeads UltraPure (Miltenyi Biotec), and $CD11c^+$ splenic DCs were collected according to the manufacturer's protocol. 2.0 x 10^5 of splenic DCs were plated in 96 well plate and the pulsed with 1.0 μM of H-2^b-restricted $OVA_{323-339}$ peptide (GenScript) for 1 h at 37°C. After washing 2 times, p-OVA-pulsed splenic DCs were co-cultured with 1.0 x 10^6 of naïve splenic $CD4^+$ T cells, which were isolated by CD4+ T cell Isolation Kit (Miltenyi Biotec) and then labeled with CellTrace Violet Cell Proliferation dye (Invitrogen). In this co-culture setting, 4A-MPLA was simultaneously added, and T cell proliferation was assessed after 72 h via flow cytometry.

T helper cell Polarization with DCs

Both DCs and naïve $CD4^+$ T cells were isolated from the spleen of B6 SPF WT (male or female, 6-8 weeks old) as described in the previous section above. Effects of synthetic lipid A analogs on $CD4^+$ T_H differentiation (T_H1, T_H2, T_H17, Treg, and Tr1) were evaluated based on the production of lineage-specific cytokines (IFN-γ, IL-4, IL-17A, and IL-10) or the expression of lineage-specific transcription factor (Foxp3) in DC-T cell co-culture setting under each polarizing condition based on previously reports.[84,85]

RORγt$^+$ Treg Polarization

For RORγt$^+$ Treg polarization, splenic DCs isolated from naïve B6 SPF WT mice (male or female, 6-8 weeks old) were co-cultured with naïve splenic $CD4^+$ T cells (DC:T cell ratio, 1:5) in the presence of antibody mixture, anti-mouse CD3 mAb (1.0 μg/mL), anti-mouse CD28 mAb (1.0 μg/mL), anti-mouse IFN-γ mAb (1.0 μg/mL), anti-mouse IL-4 mAb (1.0 μg/mL), plus *all-trans* retinoic acid (500nM) for 72 h. Different synthetic lipid A analogs (with or without 1.0 μg/mL of *Bacteroides* LOS) were initially added to this co-culture, and the proportion of RORγt$^+$ Helios$^-$ Tregs within the Tregs (Foxp3$^+$) were examined by flow cytometry.

Gut Prep

Luminal contents were pushed out with forceps and then further removed from the harvested colon by repeated flushing with sterile PBS. Colon tissues were longitudinally opened to expose the lumen and then cut into 2-3 cm pieces. Tissues were stirred with a magnetic bar in the presence of 30 mL extraction medium made with serum-free RPMI 1640 with 5.0% DTT (Sigma-Aldrich), 0.5 M EDTA (Gibco), and 2.0% FBS (Gibco) at 37°C for 15 min. Incubated tissues were transferred to a new TC dish with a sterile PBS and swooshed to get rid of residual mucus. Rinsed tissues were rolled on a paper towel and then rewashed with fresh PBS again. Tissues were dried with a paper towel and then transferred to a sterile plastic cup with 25 mL of extraction medium made with complete RPMI 1640 (with 10% FBS), 37.5 mg of Collagenase Type II (Gibco) and 12.5 mg of Dispase (Gibco). Tissues were stirred with a magnetic bar at 37°C for 30 min. Digested tissues were filtered with 40 μm Cell Strainer and then centrifuged at 2,500 rpm for 20 min at 4°C. After removing supernatant, the pellets were layered on 40%/80% Percoll (Cytivia) density gradients. The viability of isolated cells was examined by staining with Live/Dead Fixable Dead Cell Stain Kit (Invitrogen).

In vivo Examination of IFN-β Production from DCs and RORγt$^+$ APC subset

Naïve B6 SPF IFNβ1-EYFP reporter mouse (male or female, 6-8 weeks old) was orally administrated with different lipid A analogs (100 μg per mouse) and then sacrificed at different time points for examining IFN-β production from different DC subsets in the colon lamina propria. Isolated cells were stimulated with PMA (5.0 ng/mL) and Ionomycin (500 ng/mL) in the presence of protein transport inhibitors (Brefeldin A and Monensin) (BD Biosciences) for 4 h at 37°C. Stimulated cells were fixed/permeabilized and then stained with flow antibodies targeting DC phenotypic markers to distinguish cDC1, cDC2, and pDCs. Detailed information on gating strategy for flow cytometric analysis can be found in Figure S4C. For depletion of established microbiota, the antibiotics cocktail, Vancomycin hydrochloride (0.5 g/L) (ThermoFisher Scientific), Neomycin (1.0 g/L) (Millipore Sigma), Metronidazole benzoate (0.25 g/L) (AstaTech), and Ampicillin (1.0 g/L) (Millipore Sigma), is dissolved in drinking water. Same oral treatment regimen was used to examine IFN-β production in colonic RORγt$^+$ APC subset in IFNβ1-EYFP reporter mouse. The proportion of IFN-β$^+$ within the MHCII$^+$ RORγt$^+$ cells (gated on Live $CD45^+$ $TCR\beta^-$ $TCR\gamma\delta^-$ $CD19^-$ $B220^-$ $NK1.1^-$ $CXCR6^-$ Siglec-F^- $CD64^-$ Ly-$6C^-$ cells) as described in the previous report.[62]

Please cite this article in press as: Cho et al., Structure of gut microbial glycolipid modulates host inflammatory response, Cell (2025), https://doi.org/10.1016/j.cell.2025.05.016

Lipid A Analog Oral Administration and DSS-induced Colitis

Various lipid A analogs were orally administered daily from D-3 to D0 (20 μg x 4 times, total 80 μg/mouse) to B6 SPF WT (male or female, 6-8 weeks old) in prior to the treatment with 3.0% DSS-dissolved water for 7 days. Weight changes were monitored daily, and the mice were sacrificed at the end of DSS treatment for flow cytometric analysis of gut immune cells. Colon histopathology was examined by the Dana-Farber/Harvard Cancer Center Rodent Histopathology Core Facility. Colitis score was evaluated by the severity of colon inflammation. Scoring criteria is as following: 0, normal; 1, very mild colitis; 2, mild colitis; 3, moderately severe colitis; 4, severe colitis.

Lipid A-coated Latex Bead Endocytosis Assay

For coating of lipid A analogs onto the beads, Fluoresbrite YG Carboxylate Microshpheres, 1.0 μm size (Polysciences) were resuspended in PBS and incubated with various lipid A analogs (1.0 μg/mL) for overnight at 4°C in PBS. After washing 10 times with PBS containing 0.5% BSA, lipid A-coated beads were added to BMDC (1.0×10^6) isolated from B6 SPF WT (male or female, 6-8 weeks old) for 1 h at 37°C. Heterogenous patterns of bead uptake in BMDCs shown as multiple peaks on the histogram were analyzed by examining the area of subpopulation (P1-4) reflecting the DC populations having different amount of endocytosed beads (Figures S5E and S5F).

TLR4 Endocytosis Assay

As previously described,[37–39] TLR4 endocytosis was evaluated by examining the loss of TLR4 expression on BMDCs isolated from B6 SPF WT mice (male or female, 6-8 weeks old). Surface TLR4 expression was detected using a monoclonal antibody (clone MTS510, BioLegend) that specifically recognize monomeric TLR4 but not dimerized TLR4. The amount of loss of expression detected by this antibody considered to be the amount of endocytosed TLR4 upon lipid engagement in DCs.

Intracellular pH Determination

Changes in intracellular pH of BMDCs isolated from B6 SPF WT mice (male or female, 6-8 weeks old) treated with synthetic lipid A analogs was estimated by using pHrodo™ Green AM pH indicator dye (Invitrogen). Intracellular pH of BMDC was determined based on the standard curve generated from the fluorescence from 4 different pre-calibrated buffers (Buffer A to D) that are ranging from pH 4.5 to 7.5 in Intracellular pH Calibration Buffer Kit (Invitrogen).

Treatment of Endocytosis Blockers

Different chemical inhibitors (listed in Table S4) targeting different molecular mechanisms of endocytosis were treated in varying concentrations (Figures S6A–S6C) near or lower than the IC_{50} disclosed in the manufacturer's datasheet. Their impacts on IFN-β response induced by either 4A-MPLA or 6A-DPLA (Avanti Lipids) were evaluated compared to the IFN-β activity displayed in untreated control.

LD Staining and Treatment of LD Inhibitor

Lipid A analog-treated DCs (in 96 well plate) were washed with PBS 2 times and then resuspended in PBS containing 2.0 μM BODIPY 493/503 (Invitrogen). Cells were incubated for 15 min at 37°C in the dark and then washed with PBS 3 times. The kinetics of intracellular LD formation based on fluorescence intensity of BODIPY 493/503 was examined by flow cytometry. To inhibit LD biogenesis, AZD 3988 (Tocris Bioscience) was treated to DCs when DCs were initially stimulated with lipid A analogs. Functional impact of AZD 3988 on lipid A-induced IFN-β response was evaluated compared to the IFN-β activity displayed in untreated control.

Microbial Strains

Escherichia coli K12, *Bacteroides fragilis* NCTC 9343, *Bacteroides caccae* ATCC 43185, *Bacteroides cellulosilyticus* DSM 14838, *Bacteroides dorei* DSM 17855, *Bacteroides finegoldii* DSM 17565, *Bacteroides nordii* CL02T12C05, *Bacteroides ovatus* ATCC 8483, *Bacteroides salanitronis* DSM 18170, *Bacteroides salyersiae* CL02T12C01, *Bacteroides thetaiotaomicron* ATCC 29148, *Bacteroides uniformis* ATCC 8492, *Bacteroides vulgatus* ATCC 8482, *Bacteroides xylanisolvens* CL30T12C04 were individually first streaked onto Remel™ Brucella agar plates with 5% Sheep Blood, Hemin, and Vitamin K, and a single colony was inoculated into 10 mL of deoxygenated rich medium (2% proteose peptone, 0.5% yeast extract, 0.5% NaCl supplemented with 0.5% D-glucose, 0.5% K_2HPO_4, 0.05% L-Cysteine, 5 mg/L Hemin, and 2.5 mg/L vitamin K) in an anaerobic chamber (10% H_2, 10% CO_2, and 80% N_2) at 37°C. For genetic manipulation of *B. fragilis*, recombinant vectors were generated using NEB HiFi DNA Assembly Cloning Kit. During cloning procedures, *B. fragilis* were grown in Brain Heart Infusion (BHI) broth (3.7% BHI powder supplemented with 5.0 mg/L Hemin and 2.5 mg/L Vitamin K) or BHI agar plates (3.7% BHI powder and 1.5% agar supplemented with 5.0 mg/L Hemin and 2.5 mg/L Vitamin K). For bacterial selection, liquid media and agar plates were supplemented with the following combination of antibiotics: erythromycin (10 μg/mL), gentamycin (200 μg/mL), and anhydrotetracycline hydrochloride (50 ng/mL). *B. fragilis* NCTC 9343 mutants were constructed with a counterselection vector pLGB13, a gift from Laurie Comstock (University of Chicago). Overexpression of BF0187 gene in *B. fragilis* acapsular strain (*ΔungD1 ΔungD2 ΔPSH*)[65] was constructed with a chromosome-integrated and inducible vector pNBU2 erm-TetR-P1T_DP-GH023, a gift from Andrew Goodman (Yale University).[83] Disruption or integration of the targeted locus was confirmed by PCR.

Please cite this article in press as: Cho et al., Structure of gut microbial glycolipid modulates host inflammatory response, Cell (2025), https://doi.org/10.1016/j.cell.2025.05.016

LPS/LOS Extraction

The hydrolysis of bacterial LPS/LOS was carried out at mild acidic conditions. LPS/LOS was prepared in 10 mg/mL concentrations by dissolving with a 1:1 ratio of water and 100 mM sodium acetate buffer (pH 3.8-4.2). Then, LPS/LOS solution was incubated at 100°C for 3 h. Lipid A was extracted from the solution using the method previously described[86] for UHPLC-MS/MS analysis.

METHOD DETAILS

UHPLC-MS/MS

An UHPLC-MS/MS system (Thermo Scientific Vanquish RP-UPLC and Q Exactive Orbitrap) was used for bacterial lipid A profiling. Negative ion mode method was established with the following parameters: spray voltage, 3.25 kV; sheath gas, 40 AU; auxiliary gas, 8 AU; capillary temperature, 350°C; Aux gas heater temperature, 350°C; S-lens RF level, 65.0 AU; mean collision energy, 30 AU. YMC-Triart C18 column (2.1 mm x 100 mm x 3.0 μm, 200 μL/min) was used for the gradient liquid chromatography elution: 60% 2-propanol / 10% acetonitrile / 0.1% formic acid (0-2 mins), linearly increased to 85% 2-propanol / 10% acetonitrile / 0.1% formic acid (2-12 mins), held (12-24 mins), and then returned to the initial condition for 0.1 min, and held for 5.9 min at 40°C. A high-resolution (R=70,000 @ m/z 200) MS1 scan was acquired from 1000 to 2500 m/z. Top 3 data-dependent acquisition (R=17,500 @ m/z 200, isolation window: 2.0 m/z) was applied for obtaining MS/MS spectra.

Synthetic Lipid A Analog Characterization

All synthetic lipid A analogs were prepared by modified procedures from the previous reports.[87–89] The final compounds were characterized by MALDI-TOF mass spectroscopy. MALDI-TOF experiments were performed by using an UltrafleXtreme (Bruker). The sample was mixed with matrix solution (saturated pyrene solution in tetrahydrofuran). The mixture sample was spotted on MALDI target plate, and the spectra were acquired in both negative and positive polarity, reflectron mode.

Cytokine Profile Analysis

BMDCs isolated from naïve B6 SPF WT mice (male or female, 6-10 weeks old) were incubated with different lipid A analogs, and their cultured supernatants were harvested at different time points. The production of various cytokines was examined by the Mouse IL-6, IL-10, TNF-α, and IFN-β Quantikine ELISA Kit (R&D Systems) according to the manufacturer's instructions.

Lipid A Binding Assay

Recombinant human TLR4/MD2 complex protein tagged with 6x histidine (R&D Systems) were immobilized on the Ni-NTA HisSorb Plate (Qiagen) in PBS for 1 h at 37°C and then for overnight at 4°C. After washing 3 times with ELISA washing Buffer (TBS + 0.05% Tween 20), the plates were blocked with ELISA blocking buffer (PBS + 2.0% BSA) for 2 h at 37°C and the washed 3 times. Lipid A analogs reconstituted in PBS with 0.05% Tween 20 were treated with varying concentrations (10 to 1000 nM) and the incubated for 1 h at 37°C. After washing 3 times, anti-Lipid A (Abcam) was treated for 1 h at 37°C and then washed. Finally, each well was treated with anti-mouse IgM HRP for 1 h at 37°C, washed 3 times, developed with TMB Substrate (Invitrogen), and then quenched with STOP Solution (0.18 M H_2SO_4).

Transcriptomic Analysis

Bulk RNA-Seq analysis performed on the O2 High Performance Compute Cluster supported by the Research Computing Group at HMS (see http://rc.hms.harvard.edu for more detailed information). The FASTQ files were inspected using FastQC and Qualimap for the QC of sequencing reads. The QC-passed reads were then mapped to the moused genome (mm10 genome assembly) using STAR Aligner. All lanes of the aligned reads were combined and then sorted using SAMTools. The sorted reads were counted using HTSEQ Count using their name and union flags. Finally, the gene expression count files were processed using DESeq2 to determine which genes were differentially expressed. Once the read files were processed through the RNA-Seq analysis pipeline, they were further analyzed using R (v4.3.1). Statistics needed to generate the plots used in the analysis were obtained using DESeq2. Principal component analysis and volcano plots were constructed using ggplot2 R package. The multidimensional scaling plot was constructed using the classical metric multidimensional scaling function, which is in the stats package and ggplot2. Heatmaps were constructed using the Gene Pattern application Morpheus.

Total RNA Extraction and q-PCR

DCs treated with lipid A analogs were harvested and centrifuged for 1 min at 18,000 rpm at 4°C. After discarding supernatant, cell pellets were treated with 500 μL of TRIzol (Invitrogen) and incubated for 5 min at RT, then for 1 h or overnight at -80°C. Thawed samples were treated with 100 μL of chloroform and then vigorously vortexed for 15 sec. After incubation at RT for 5 min, the samples were centrifuged 15 min at 18,000 rpm at 4°C, and the aqueous fractions were collected into new tubes in ice. 1.0 μL of Glycoblue Coprecipitant (Invitrogen) was treated to each tube, and 250 μL of isopropanol was treated to each sample. After incubation for 1 h at -80°C, the samples were centrifuged for 20 min at 18,000 rpm at 4°C. Supernatants were discarded, and the pellets were washed with 500 μL of 75% ice-cold ethanol. After centrifugation, the pellets were air-dried for 1 h and resuspended with nuclease-free water (Invitrogen). Total amount of RNA was quantified with NanoDrop (Thermo Scientific). cDNA was synthesized using PrimeScript RT

Reagent Kit (Takara Bio) according to the manufacturer's protocols. q-PCR was performed by QuantStudio 5 with iTaq Universal SYBR Green Supermix (Bio-Rad) and the set of qPCR primers (each sequence can be found in the key resources table). Each gene expression was normalized by the expression of murine *Actb* used as a reference gene.

QUANTIFICATION AND STATISTICAL ANALYSIS

All statistical analyses were performed using Prism software (version 10.5.0, GraphPad). Paired or unpaired Student's t tests were used as appropriate. Significance was defined as follows: n.s., not significant; *, $p < 0.05$, **, $p < 0.01$, *** $p < 0.001$.

Supplemental figures

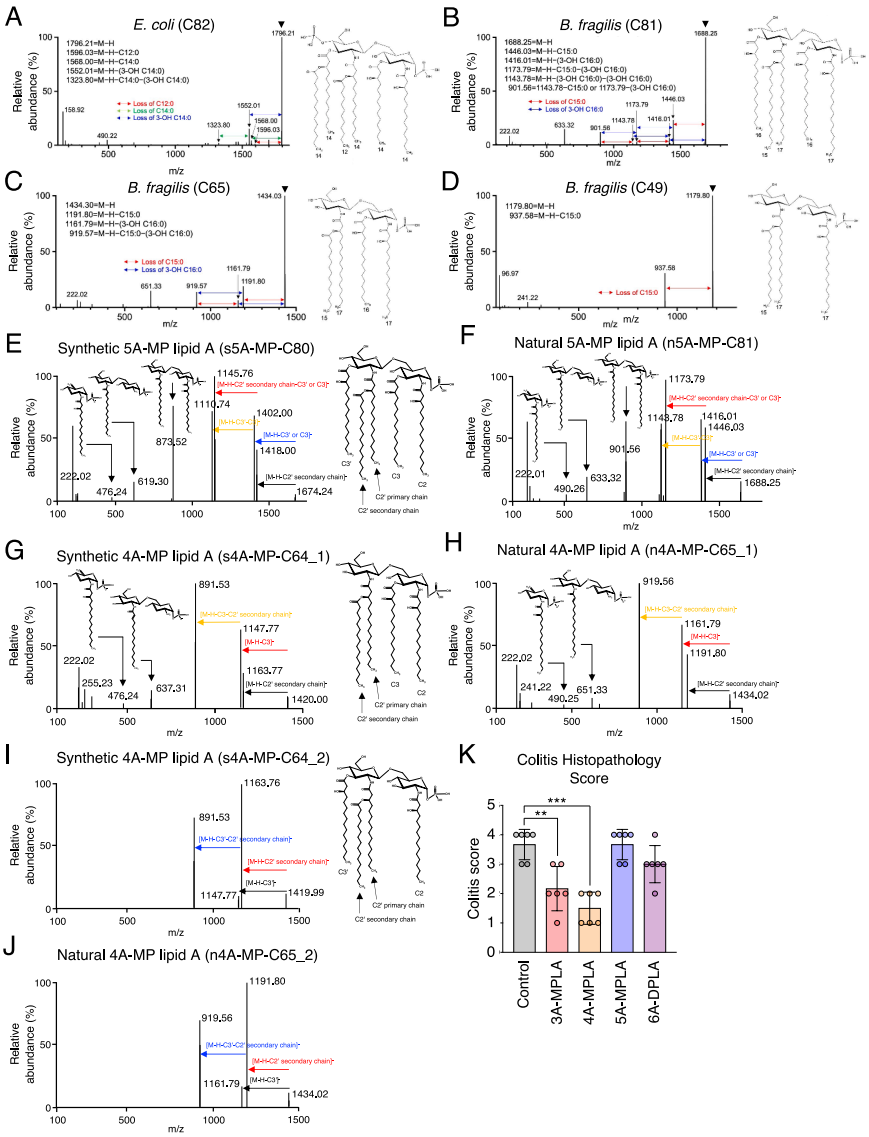

Figure S1. Structural assignment of natural lipid A species in *E. coli* and *B. fragilis* and colitis histopathology assessment, related to Figure 1

(A–D) Detailed analysis of lipid A structures found in *E. coli* Nissle 1917 (A) and *B. fragilis* having penta- (B), tetra- (C), and tri-acyl chain (D) analyzed by liquid chromatography tandem mass spectrometry (LC-MS/MS). Proposed structures of the most abundant lipid A species (the peak indicated by down arrowhead) are shown on the right.

(E–J) Comparative profile of synthetic penta- (s5A-MP-C80) (E) and tetra-acylated (s4A-MP-C64_1 and s4A-MP-C64_2) lipid A analogs (G and I) vs. natural penta- (n5A-MP-C81) (F) and tetra-acylated (n4A-MP-C65_1 and n4A-MP-C65_2) (H and J) lipid A species found in *B. fragilis*. The peaks shown in (F), (H), and (J) originate from the marked peaks in the penta-acylated (m/z 1,688.25) (B) and tetra-acylated (m/z 1,434.03) (C) lipid A species from *B. fragilis*.

(K) Colitis histopathology scored by the severity of colon inflammation. Scoring criteria is as following: 0, normal; 1, very mild colitis; 2, mild colitis; 3, moderately severe colitis; 4, severe colitis.

n.s., not significant; $*p < 0.05$; $**p < 0.01$; $***p < 0.001$, unpaired/paired Student's t test. Error bars represent mean ± SEM.

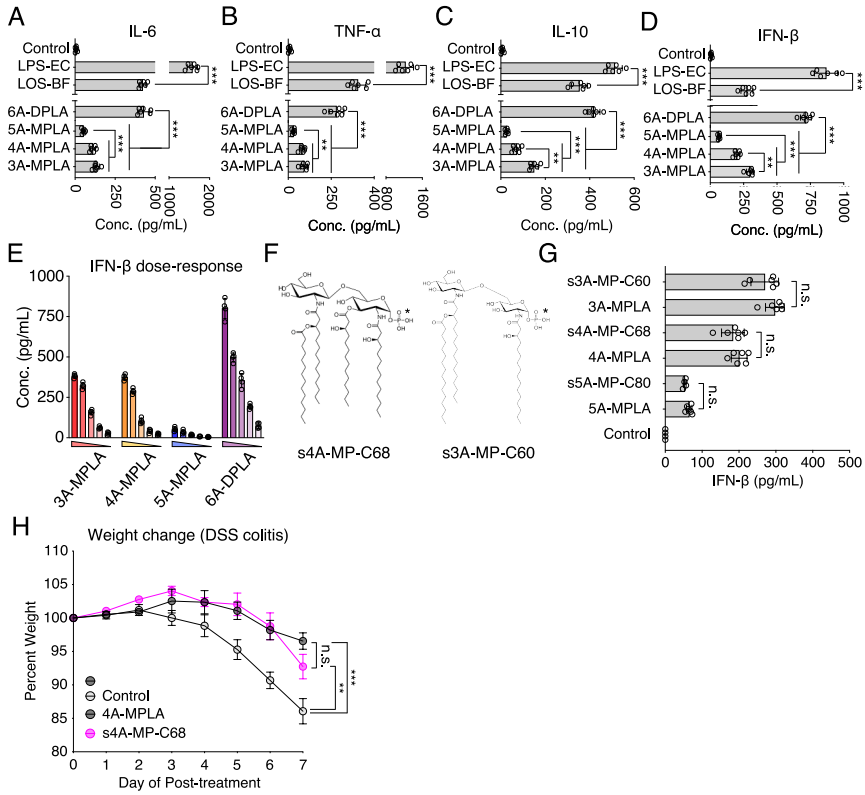

Figure S2. Cytokine responses induced by synthetic lipid A analogs and immunoprotective effect on colonic inflammation, related to Figure 2

(A–D) Cytokine responses from BMDCs stimulated by synthetic lipid A analogs (1.0 μg/mL) or bacterial LPS/LOS purified from *E. coli* (LPS-EC) or *B. fragilis* (LOS-BF) (1.0 μg/mL).

(E) IFN-β response from mBMDCs induced by different lipid A analogs in varying concentrations (5–1,000 ng/mL).

(F–H) Molecular structure of synthetic tetra-acylated (s4A-MP-C68, left) and tri-acylated (s3A-MP-C60, right) lipid A analogs containing a single C1 phosphate (C1P, highlighted with an asterisk). Structure of synthetic penta-acylated (s5A-MP-C80) lipid A analog with C1P is shown in Figure S1E (F). Comparative IFN-β response between synthetic 3A- to 5A-MPLA and their C4′P lipid A analog counterparts from BMDCs (G). Immunoprotective effect of 4A-MPLA and s4A-MP-C68 (C1P isomer to 4A-MPLA), as determined by weight changes during DSS treatment.

n.s., not significant; $*p < 0.05$; $**p < 0.01$; $***p < 0.001$, unpaired/paired Student's t test. Error bars represent mean ± SEM.

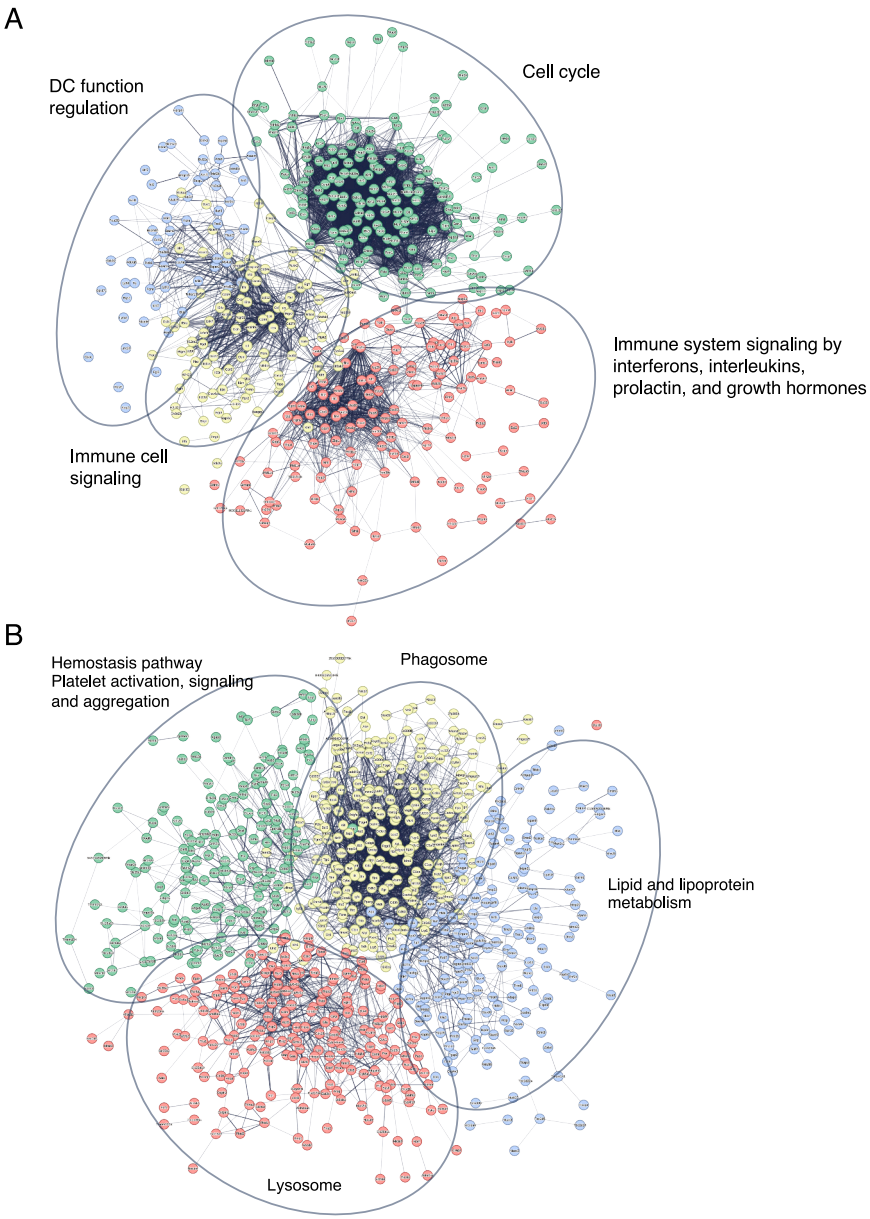

Figure S3. String analysis of upregulated/downregulated DEGs in DCs induced by 3A- or 4A-MPLA treatment compared with control, related to Figure 2

(A and B) Functional networks of DEGs (determined by DEseq2, $p_{adj} < 0.05$) that are strongly upregulated (log_2 [fold change] > 1.0) (A) or downregulated (log_2 [fold change] > 1.0) (B) by 3A- or 4A-MPLA are visualized via STRING software. List of genes in each functional cluster can be found in Tables S3 and S4.

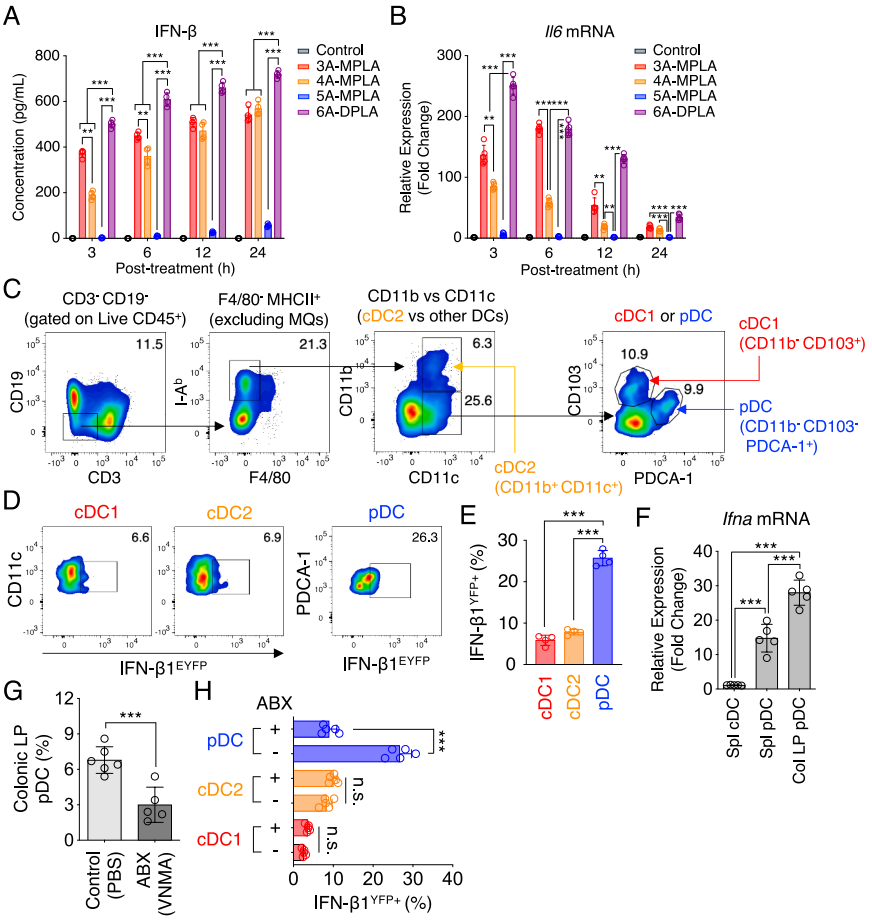

Figure S4. IFN-β and IL-6 response kinetics regulated by lipid A structures from DCs, related to Figure 3

(A) IFN-β secretion being accumulated in cultured supernatant of mBMDCs at different time points induced by different lipid A analogs.

(B) *Il6* mRNA expression kinetics at different time points in mBMDCs induced by different lipid A analogs.

(C–E) Gating strategy of flow analysis to examine IFN-β production from various DC subsets (cDC1, cDC2, and pDC) in the colon LP of IFNβ1-EYFP reporter mice after the oral administration of synthetic lipid A analogs (100 μg/mouse) (C and D). Compiled IFN-β^{EYFP+} proportions from cDC1, cDC2, and pDC from colon LP of IFNβ1-EYFP reporter mice treated with PBS (control) (E).

(F) *IFNa* mRNA expression from splenic cDC and pDC plus colonic pDC of WT B6 mice.

(G and H) Effect of microbiota depletion by administration of antibiotics (ABX, vancomycin, neomycin, metronidazole, and ampicillin cocktail) on the proportion of colonic pDC (G) and IFN-β production by different colonic DC subsets from IFN-β1-EYFP reporter mice (F).

n.s., not significant; *$p < 0.05$; **$p < 0.01$; ***$p < 0.001$, unpaired/paired Student's t test. Error bars represent mean ± SEM.

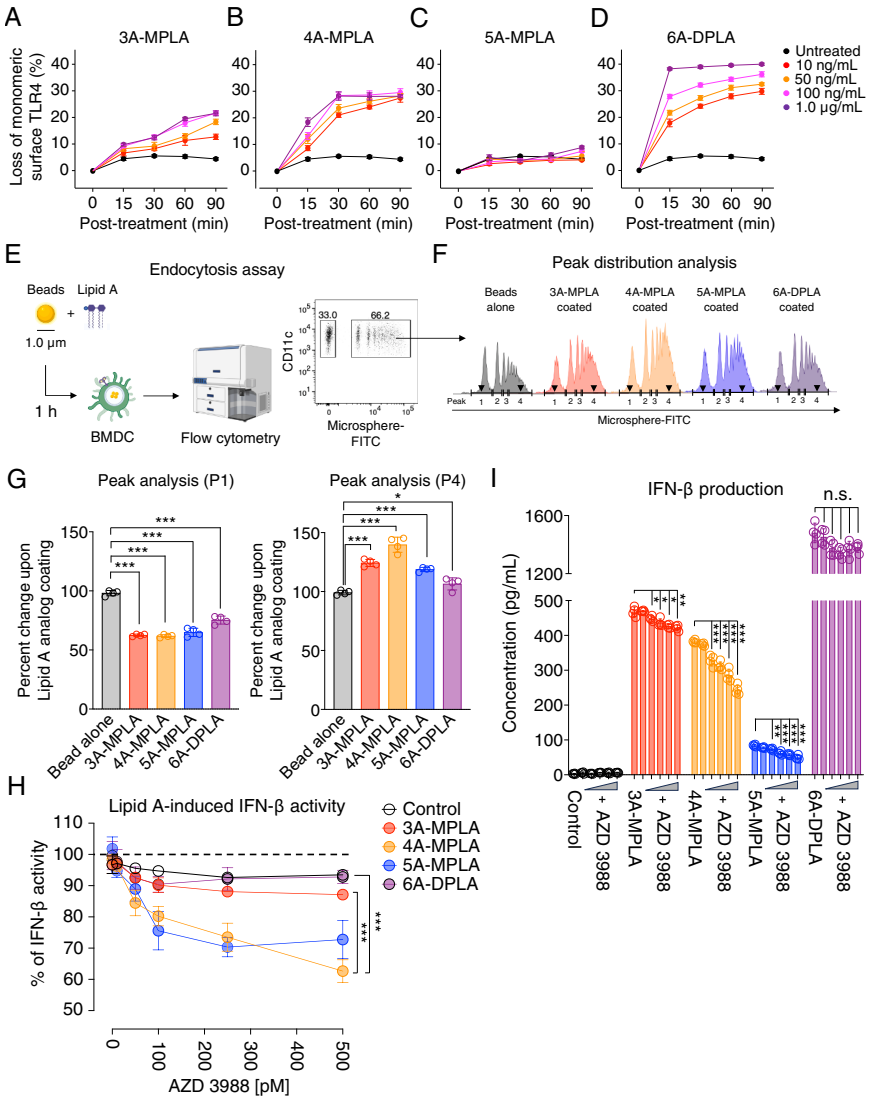

Figure S5. Synthetic lipid A analog-induced endocytosis and impact of LD inhibitor on lipid A-induced IFN-β response, related to Figure 3

(A–D) Percentage loss of monomeric TLR4 expression on the surface in response to varying concentration of synthetic lipid A analogs (10–1,000 ng/mL) to mBMDCs at indicated time points.

(E–G) Experimental scheme of endocytosis assay using Fluoresbrite Yellow/Green carboxylate microspheres (1.0 μm) surface coated with different synthetic lipid A analogs in mBMDCs via flow cytometric analysis (E). Histograms of microsphere-endocytosed CD11c$^+$ DCs after 1 h post treatment. Microsphere-endocytosed DCs were analyzed based on the fluorescence intensity of shown peaks (P1–P4) in the histogram reflecting relative amounts of endocytosed beads in the cells. The peaks showing the lowest (P1) and highest (P4) fluorescence intensity in the histogram are indicated by down arrowheads (F). Percent changes in P1 and P4 subpopulations following treatment of lipid A analog-coated latex beads, compared with control beads without lipid A (G).

(H and I) Lipid A-induced IFN-β activity inhibited by varying concentrations of DGAT1 (diacylglycerol O-acyltransferase 1) inhibitor AZD 3988 (10–500 pM). Dotted line on the graph indicates the uninhibited IFN-β activity (%) induced by each synthetic lipid A analog (1.0 μg/mL) in the absence of AZD 3988 (H). Measured concentration of IFN-β from the cultured supernatant of BMDCs stimulated with synthetic lipid A analogs with or without AZD 3988 (I).

n.s., not significant; *$p < 0.05$; **$p < 0.01$; ***$p < 0.001$, unpaired/paired Student's t test. Error bars represent mean ± SEM.

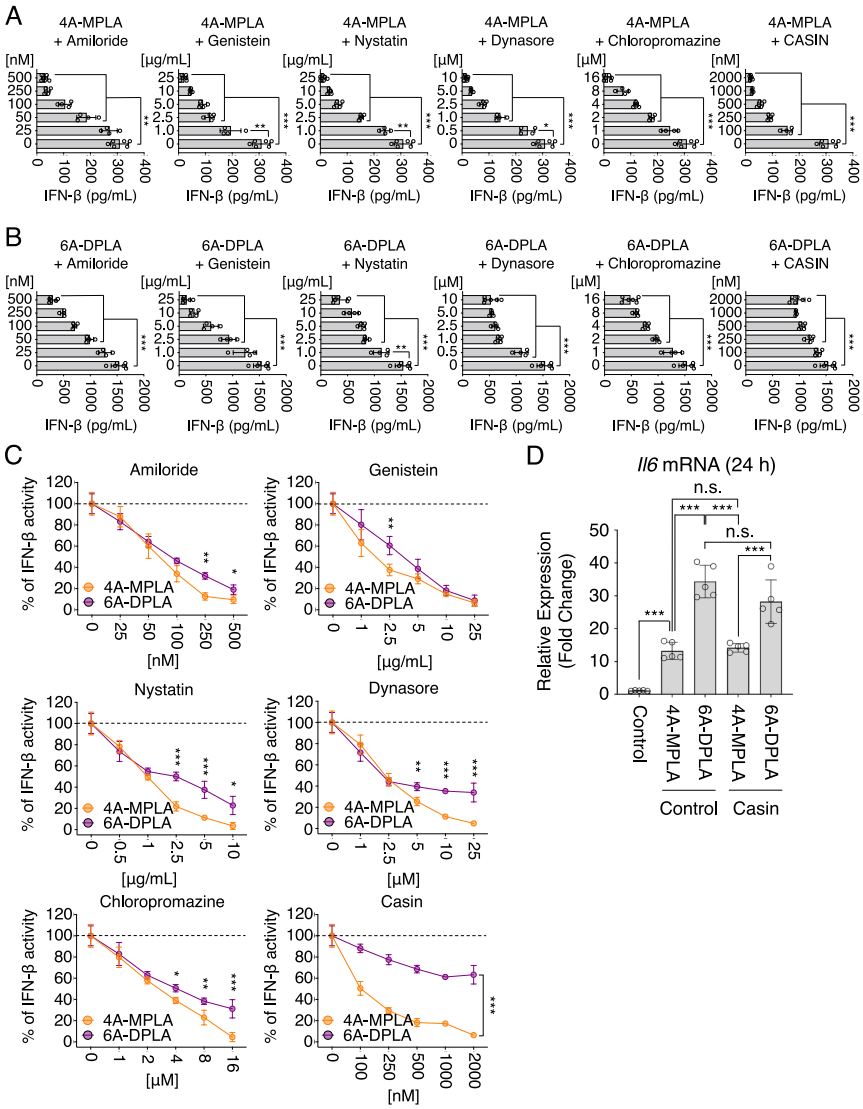

Figure S6. Effect of various endocytosis inhibitors on lipid A-induced IFN-β and IL-6 responses, related to Figure 4

(A and B) Measurement of IFN-β production induced by 4A-MPLA or 6A-DPLA (1.0 μg/mL) in mBMDCs in the presence of amiloride (25–500 nM), genistein (1.0–25 μg/mL), nystatin (1.0–25 μg/mL), dynasore (0.5–10 μM), chloropromazine (1.0–16 μM), and CASIN (100 nM–2 μM).

(C) Lipid A-induced (4A-MPLA vs. 6A-DPLA) IFN-β activity inhibited by varying concentrations of endocytosis inhibitors. Dotted line on the graph indicates the uninhibited IFN-β activity induced by 4A-MPLA or 6A-DPLA with no inhibitors.

(D) *Il6* mRNA expression at 24 h post treatment of 4A-MPLA or 6A-DPLA in the presence or absence of 500 nM CASIN (Cdc42 inhibitor), examined by qPCR. n.s., not significant; *$p < 0.05$; **$p < 0.01$; ***$p < 0.001$, unpaired/paired Student's t test. Error bars represent mean ± SEM.

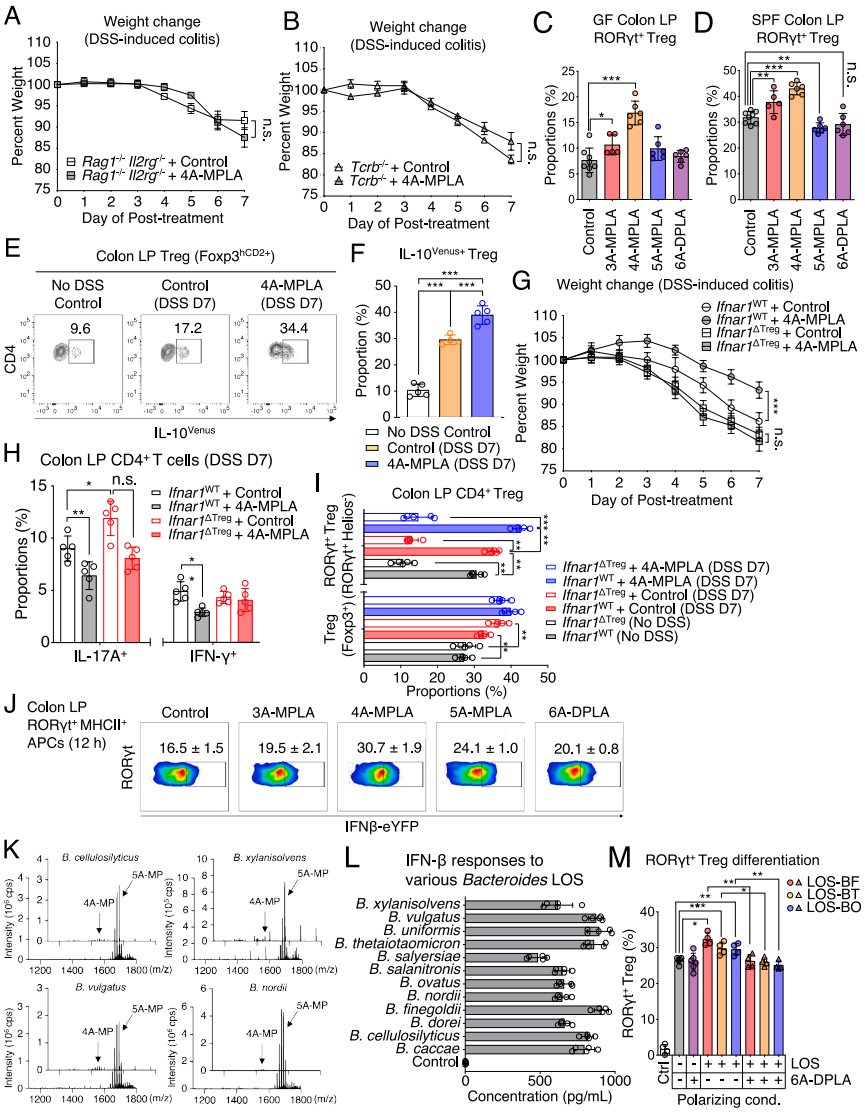

Figure S7. Effect of 4A-MPLA and *Bacteroides* LOS on RORγt$^+$ Tregs and colonic inflammation, related to Figure 6

(A and B) Immunoprotective effect of 4A-MPLA on DSS-induced colitis in *Rag1*$^{-/-}$ *Il2rg*$^{-/-}$ (A) and *Tcrb*$^{-/-}$ (B) determined by weight changes during DSS treatment.

(C and D) Impact of lipid A analog oral administration on colonic RORγt$^+$ Tregs from GF (C) and SPF B6 WT mice (D) under the steady-state conditions. Lipid A analogs (20 μg) were administered daily for 4 days (total 80 μg/mouse). Compiled proportions of RORγt$^+$ Helios$^-$ Tregs within the colonic LP Foxp3$^+$ Tregs are shown.

(E and F) Proportion of IL-10-producing Tregs (IL-10^{Venus+}) in the colon of B6 *Foxp3*^{hCD2} × *Il10*^{Venus} dual reporter mice in the steady-state (no DSS control) or during DSS-induced colitis (DSS day 7) treated with or without 4A-MPLA.

(G–I) Immunoprotective effect of 4A-MPLA on DSS-induced colitis in *Foxp3-cre* × *Ifnar1*$^{+/+}$ (*Ifnar1*^{WT}) or *Ifnar1*$^{f/f}$ (*Ifnar1*$^{\Delta Treg}$) determined by weight changes during DSS treatment (G), colitogenic cytokine production (IL-17A and IFN-γ) from colon LP CD4$^+$ T cells (H), and Tregs (Foxp3$^+$) and RORγt expression within Tregs (RORγt$^+$ Helios$^-$) at day 7 post DSS treatment (DSS day 7) or no DSS control (I).

(J) Impact of lipid A analog oral administration on IFN-β induction (at 12 h post treatment) in the colonic RORγt$^+$ MHCII$^+$ APCs (gated on Lin$^-$ Ly6C$^-$ CD64$^-$ cells, detailed gating strategy described in the methods) using IFNβ1-EYFP reporter mice (B6.129-*Ifnb1*^{tm1Lky}/J). The proportions of IFN-β$^+$ cells within the RORγt$^+$ MHCII$^+$ APCs are represented as mean ± SD. The same treatment regimen used in Figure S4C was used in this experiment.

(K) Lipidomic profile of other *Bacteroides* species (*B. cellulosilyticus*, *B. xylanisolvens*, *B. vulgatus*, and *B. nordii*).

(L) IFN-β response from the mBMDCs induced by the LOS molecules isolated from various *Bacteroides* species.

(M) Effect of 6A-DPLA (5.0 μg/mL) on RORγt$^+$ Treg differentiation in the presence of various *Bacteroides* LOS (1.0 μg/mL) under the *in vitro* polarization condition. The LOS were individually isolated from *B. fragilis* (LOS-BF), *B. thetaiotaomicron* (LOS-BT), and *B. ovatus* (LOS-BO).

n.s., not significant; *$p < 0.05$; **$p < 0.01$; ***$p < 0.001$, unpaired/paired Student's t test. Error bars represent mean ± SEM.